Chalmers University of Technology

Numerical Investigation of Hydrogen Combustion in a Micromix Combustor for Industrial Gas Turbine Applications

Master's thesis in Innovative and Sustainable Chemical Engineering

Nattha Apairat

DEPARTMENT OF CHEMISTRY AND CHEMICAL ENGINEERING

CHALMERS UNIVERSITY OF TECHNOLOGY
Gothenburg, Sweden 2024
www.chalmers.se

Master's thesis 2024

Numerical Investigation of Hydrogen Combustion in a Micromix Combustor for Industrial Gas Turbine Applications

Nattha Apairat

CHALMERS
UNIVERSITY OF TECHNOLOGY

Department of Chemistry and Chemical Engineering
Division of Chemical Engineering
Chalmers University of Technology
Gothenburg, Sweden 2024

Numerical Investigation of Hydrogen Combustion in a Micromix Combustor for Industrial Gas Turbine

NATTHA APAIRAT

Supervisor: Dr.Daniel Moëll, Siemens Energy AB
Examiner: Prof.Ronnie Andresson, Chalmers University of Technology

Master's Thesis 2024
Department of Chemistry and Chemical Engineering
Chalmers University of Technology
Sweden
SE-412 96 Gothenburg
Telephone +46 31 772 1000

In cooperation with:
Siemens Energy AB
SE-612 31 Finspång
Sweden
Telephone + 46 122 810 00
www.siemens-energy.com

Printed by Chalmers Reproservice
Gothenburg, Sweden 2024

Numerical Investigation of Hydrogen Combustion in a Micromix Combustor for Industrial Gas Turbine Applications
NATTHA APAIRAT
Department of Chemistry and Chemical Engineering
Chalmers University of Technology

Abstract

Hydrogen emerges as a favorable alternative fuel for industrial gas turbines, offering the potential for zero carbon emissions. This study explores the numerical methods for modeling pure hydrogen combustion within a micromix combustor for industrial gas turbine applications. The micromix combustor is a potential design to mitigate undesired phenomena such as flashback due to the unique properties of hydrogen. Various chemical mechanisms, turbulence models, and combustion approaches are examined and compared to optimize simulation accuracy and computational efficiency. Strategic domain generation and mesh refinement focus on critical areas around the fuel injection and mixing zones. Validation of the mesh, comprising 21 million cells, confirms its accuracy and captures asymmetry arising from inherent physics and geometry.

Among three Reynolds-Averaged Navier-Stokes (RANS) models containing LagEB $k-\varepsilon$, standard $k-\varepsilon$, and SST $k-\omega$, LagEB $k-\varepsilon$ provides the most promising results, demonstrating superior performance in predicting temperature profiles and flow fields. Chemical mechanisms, including GRI, FOI and NUIG, yield comparable results in both temperature and flow fields, with FOI selected for its computational efficiency. Comparison between RANS and Large Eddy Simulation (LES) reveals that hot spots can be observed in RANS which consequently results slightly higher exit temperature than LES. This finding underlines the advantage in mitigating the underestimation of turbulent kinetic energy dissipation. Investigation of combustion models, including Flamelet Generated Manifolds (FGM) and Laminar Flame Concept (LFC), emphasizes the influence of geometry and model complexity on simulation convergence and computational resources.

The findings highlight the significance of appropriate numerical method for predicting hydrogen combustion dynamics and offer insights into turbulence prediction and fuel-air mixing. The case applying RANS LagEB $k-\varepsilon$ with FGM model and FOI mechanism is justified as an effective model with optimal computational expense. It is capable to accurately predict flame shape, temperature, and flow fields when validating against the experiment and adiabatic flame temperature. Besides its potential, hydrogen combustion is still developing, further studies on geometry, boundary conditions, stability, and NOx formation should be considered to optimize the system and strategies for emission reduction.

Acknowledgements

This thesis was carried out at the department of combustion at Siemens Energy with the cooperation from the department of chemistry and chemical engineering, Chalmers University of Technology.

First of all I would like to thank my Industrial supervisor, Dr. Daniel Moëll, for the constructive guidance and valuable discussions through out this work. My Academic supervisor Prof. Ronnie Andresson is greatly acknowledged for the feedback and suggestions on this work. I greatly appreciate my manager Saeid Kharazmi at the department of combustion, Siemens Energy for giving me the opportunity to work on this thesis. The colleagues from Montreal, Pierre Gauthier and Antoine Durocher, are acknowledged for assisting me about the simulation set up and experimental results. All of my colleagues at Siemens Energy are immensely appreciated for being supportive and providing an incredible working environment.

I would like to send a special acknowledgement to Mr.Sievert Larsson for providing me a scholarship to pursue a master's degree in Sweden. I would not make it to be here without your support. Last but not least, I am thankful for my family and friends for always having my back.

Nattha Apairat, Finspång, June 2024

List of Acronyms

Below is the list of acronyms that have been used throughout this thesis listed in alphabetical order:

CAD	Computer-Aided Design
CFD	Computational Fluid Dynamics
CFL	Courant Friedrichs Lewy
DLE	Dry Low Emission
DNS	Direct Numerical Simulation
FGM	Flamelet Generated Manifold
FOI	Swedish Defence Research Agency
GRI	Gas Research Institute
LagEB	Lag Elliptic Blending
LES	Large Eddy Simulation
LFC	Laminar Flame Concept
NUIG	National University of Ireland, Galway
RMS	Root Mean Square
SST	Shear Stress Transport
StarCCM+	Commercial CFD software
WALE	Wall-Adapting Local-Eddy Viscosity

Nomenclature

Below is the nomenclature of indices, sets, parameters, and variables that have been used throughout this thesis.

Greek letters

α	Elliptic blending factor	
ε	Turbulence dissipation rate	$[m^2/s^3]$
η	Kolmogorov length scale	$[m]$
λ	Taylor microscale	$[m]$
μ	Dynamic viscosity	$[Pa \cdot s]$
μ_t	Turbulent viscosity	$[Pa \cdot s]$
ν	Kinematic viscosity	$[m^2/s]$
ξ	Mixture fraction	
ρ	Density	$[kg/m^3]$
τ	Viscous stress tensor	$[Pa]$
ϕ	Transport variable	
φ	Wall normal stress component	$[Pa]$
ω	Specific dissipation rate	$[s^{-1}]$
Δ	Filter width (element size)	$[m]$

Latin letters

c	Reaction progress	
c_p	Specific heat capacity	$[J/(Kg \cdot K)]$
C	Chemicl species vector	$[mol/m^3]$
D	Diffusivity	$[m^2/s]$
Da	Damkohler number	

f	Mean reaction rate multiplier	
F	Diffusion flux	$[kg/(m^2 \cdot s)]$
g	Body force per volume	$[N/m^3]$
h	Enthalpy	$[J/Kg]$
I	Identity matrix	
k	Turbulent kinetic energy	$[J/Kg]$
l	Turbulent length scale	$[m]$
L	Characteristic length	$[m]$
p	Instantaneous pressure	$[N/m^2]$
Re	Reynolds number	
S	Strain rate tensor	$[s^{-1}]$
S_w	Deformation parameter	

Superscript

$\overline{\phi}$	Filtered value
ϕ'	Subgrid value

Subscript

i, j, k	Cartesian coordinate direction on x, y, z axis
res	Resolved
SGS	Subgrid scale
SST	SST model

Contents

List of Figures

List of Tables

1

Introduction

This chapter presents the global energy consumption and reduction of carbon emission trends along with the influence of hydrogen to be used as an alternative fuel in gas turbine. Problem formation, objectives, and limitations of this study are discussed in this chapter.

1.1 Background

The energy demand has been increased remarkably over the past centuries as a result of population growth, economic development and urbanization. According to the World Energy Outlook [1], three different scenarios to explore the uncertainties affecting the energy transition to 2050 are examined. The scenarios include Accelerated, Net Zero and New Momentum. The scenarios consider carbon emission from energy production and utilization. Accelerated and Net zero investigate how the changes in energy system might contribute to decreasing in CO_2-equivalent emissions to drop by 75% by 2050 relative to 2019 level for Accelerated and 95% for Net Zero. A range of possible pathways of global energy system to 2050 is shown in Figure 1.1.[1]. The assumption of significant restricting of climate policies is applied for Accelerated and Net zero.

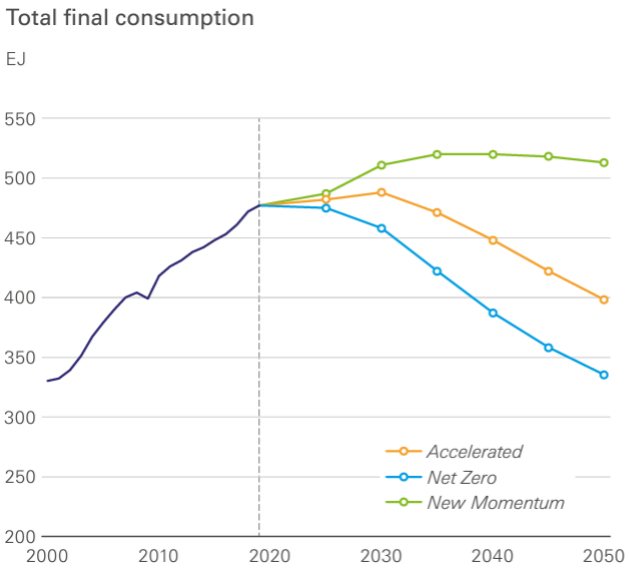

Figure 1.1: Global energy consumption in different scenarios.

The annual Statistic Review of World Energy indicates that while renewable power expended rapidly, fossil fuels maintained an 82% of total primary consumption and carbon dioxide emissions from energy rose to a new high of 34.4 billion metric tons in 2023 [1]. Carbon dioxide is one of the most abundant greenhouse gases which significantly contributes to global warming. According to the Paris agreement, the global temperature change needs to be limited below 2℃[2]. The finite quantity of energy demand and mission for decarbonization have led the research institutes and power producing industry into the development of alternative sustainable energy generation aiming to reduce the emissions in particular Carbon dioxide and Nitrogen oxides.

Gas turbines are considered as a dominant technology to produce energy worldwide and it is normally fueled with natural gas or liquid fuel. Combustion of these hydrocarbons results in CO_2 and NOx emissions. Alternative fuels with high hydrogen content are as importance for a sustainable future power plant development. Hydrogen serves as a promising alternative fuel for several compelling reasons. Hydrogen combustion does not emit CO_2 and it may act as energy storage by using the excess energy from renewable energy sources such as wind or solar power to produce green hydrogen through water electrolysis [3].

However, current well-established gas turbines cannot be directly operated with hydrogen combustion due to the differences in physical properties compared to hydrocarbon fuels. The technology for dry and low emissions (DLE) in combustors have been developed and implemented in gas turbines by the lean premixed method to reduce the flame temperature and lowering NOx emission [4]. Premixing may not be suitable for hydrogen because of its high reactivity and diffusivity. These proper-ties may cause the local flame speed to be higher than the local flow speed allowing the flame to propagate upstream to the unburnt mixture. This is the flash back. The higher flame temperature and local heat release also promote NOx formation. Therefore, the strategies to handle the risk of flash back and reduce pollution are crucial and challenging.

1.2 Problem formation

Regarding operational and environmental concern, an investigation to further increase fuel flexibility and capability to further expand the usage of green fuels is important. The most challenging green fuel for dry low emission combustion is hydrogen due to its high reactivity moving the flame upstream causing risk of excessive heat load on the burner. Moreover, high flame temperature causes the NOx formation to be pronounced. In this thesis, micro diffusion flames for pure hydrogen operation in gas turbines is investigated using CFD simulations by use of StarCCM+. The suitable simulation methods were examined using academic test case. First focus is on predictions on flame shapes and flame temperatures.

1.3 Objectives

- To identify suitable numerical methods to predict the micro diffusion flame of pure hydrogen combustion in a gas turbine using a micromix combustor in the academic test case.
- To examine mesh sensitivity and ensure mesh independent solutions.
- To investigate the effect of using different chemical kinetics schemes, turbulence and combustion models on pure hydrogen combustion.
- To perform first CFD assessment of gas turbine system with pure hydrogen and micro diffusion flames and recommend suitable burner geometry.

1.4 Limitations

- Since the application has complex geometry and turbulence model such LES require heavy computation, the results are limited by the computational resources and time span for this thesis.
- The combustion methods are limited to micro diffusion flames.
- The validation of flame temperature from the simulations against the experiments are restrained by limitation of the temperature measurement accuracy from the experiments.

2
Theory

This chapter provides the necessary background, introduction and fundamental theory required to understand the investigation of hydrogen combustion in gas turbine. Initially, a broad overview of gas turbines and their principal components are described. After that, the principles of fluid dynamics is explained followed by basic theories within combustion and reacting flow.

2.1 Gas Turbine

An industrial gas turbine is a combustion engine that transforms natural gas or other alternative fuels into mechanical energy for various applications. Its key components include a compressor, a combustion chamber, and a turbine. The operation of an industrial gas turbine involves intake, compression, combustion, expansion, and power generation stages. Intake draws air into the compressor, where it is pressurized before entering the combustion chamber. Fuel is injected and ignited in the combustion chamber, generating hot gases that expand through the turbine, driving its rotation. This rotation powers the generator, producing electricity. Industrial gas turbines find applications in power generation for industrial, commercial, and residential sectors, as well as in the oil and gas industry for equipment propulsion and electricity generation. They are also utilized in aviation as aircraft engines and in marine propulsion systems for ships and other vessels [5].

2.1.1 Combustion Chamber

The combustion chamber within a gas turbine plays an important role in the energy generation process by facilitating the controlled combustion of fuel. Compressed air from the compressor stage, enters the combustion chamber where it mixes with fuel injected. This mixing occurs within a designated zone to ensure an optimal fuel-air ratio for combustion. Ignition systems, such as spark plugs or ignitors, initiate combustion, leading to the rapid release of heat energy. This process elevates the temperature and pressure of the gases within the chamber. The resulting high-temperature gases then exit the combustion chamber and flow into the turbine section, where they drive the turbine blades, ultimately generating power. Design considerations for the combustion chamber include efficient fuel utilization, minimal emissions, and reliable operation across varying conditions, all of which contribute to the overall performance and efficiency of the gas turbine system [6].

2.1.2 Hydrogen as an Alternative Fuel in Gas Turbines

Utilizing hydrogen as a fuel in gas turbines is increasingly favored due to its potential to mitigate environmental concerns and facilitate the transition to cleaner energy sources. Hydrogen combustion yields only water vapor as a byproduct, aligning with efforts to reduce greenhouse gas emissions and combat climate change. Additionally, hydrogen can be produced through electrolysis using renewable energy, offering a pathway for integrating renewable energy sources into the energy system. Its high energy density makes it an efficient fuel for power generation, enabling compact fuel storage and extended operating duration.

However, challenges exist in adopting hydrogen as a gas turbine fuel. Due to the unique combustion characteristics of hydrogen, such as its wide flammability range and high flame speed, present challenges for combustion stability and flame dynamics within the turbine. The well-established dry low emission (DLE) combustor is operated by burning the fuel at lean premixed condition to operate at a much lower temperature and thus NOx production is reduced. This means that the fuel and air need to be mixed before entering the combustion chamber. This condition is not suitable to apply directly for hydrogen due to its reactivity that might lead to flashback to the upstream burner [7]. Therefore, the modification of the combustor is necessary for hydrogen combustion.

2.1.3 Micromix Combustor

A micromix combustor is a promising combustion system designed to reduce the climate impact of gas turbine by using hydrogen as a fuel, this technology delivers zero carbon emission with potentially low NOx and combustion with significantly low risk of flashback or autoignition. It utilizes advanced mixing techniques to achieve thorough fuel-air rapid mixing in a cross flow at a small scale within the combustor and generates a multitude of small flames. This intense micromixing, facilitated by micro-scale injectors, swirlers, or turbulence inducers, ensures uniformity in the fuel-air mixture. Moreover, micromix combustors employ specialized flame stabilization techniques, such as flame holders and vortex generators, to anchor and stabilize the flame within the combustion chamber. Reducing the time taken for mixing while enhancing the intensity of mixing results in decreased emissions of pollutants. The high reactivity and wide flammability limits of hydrogen in micromix combustor can produce short and low temperature micro flames, with lean overall equivalence ratios which are a result of intense mixing without the risk of flashback. Additionally, their compact design makes them suitable for integration into gas turbine systems with limited space, enhancing overall system efficiency [8].

2.2 Modeling of Reacting Flow in Gas Turbine Combustors

2.2.1 Fundamental Governing Equations

The fundamental principles of physics and momentum conservation are the basis of all fluid dynamics modeling. Transport of mass, heat and momentum occurs by convection of the mean flow and by random motion of molecules or in turbulent flow by random movement of fluid elements. The governing equations for a turbulent reacting flow are given by the continuity in equation (2.1), the conservation of momentum in equation (2.2),the conservation of energy in equation (2.3) and the species in equation (2.4) [9] [10].

$$\frac{\partial \rho}{\partial t} + \frac{\partial (\rho u_i)}{\partial x_i} = 0 \tag{2.1}$$

In this context, i and j represent the components of a three-dimensional vector (i, j = 1, 2, 3). ρ is the mixture mass density and u is velocity vector.

$$\frac{\partial (\rho u_j)}{\partial t} + \frac{\partial (\rho u_i u_j)}{\partial x_i} = -\frac{\partial p}{\partial x_j} + \frac{\partial \tau_{ij}}{\partial x_i} + \rho g_j \tag{2.2}$$

Here p is pressure and to relate the pressure with density and temperature, the ideal gas law is applied. τ_{ij} is the viscous stress tensor, g is body forces acting on the system.

$$\frac{\partial \rho h}{\partial t} + \frac{\partial \rho u_i h}{\partial x_i} = \frac{\partial}{\partial x_i}\left(\rho \alpha \frac{\partial h}{\partial x_i}\right) + \frac{Dp}{Dt} + \tau_{ij}\frac{\partial u_j}{\partial x_i} + S_T \tag{2.3}$$

A balance for heat equation (2.3) can be formulated by adding the source terms from the kinetic-energy balance and from chemical reaction. The terms written here are for accumulation, convection, conduction, expansion, dissipation and a general source e.g. reaction enthalpy, radiation. Here h is the mixture enthalpy, α is the thermal diffusivity.

$$\frac{\partial \rho Y_i}{\partial t} + \frac{\partial \rho u_i Y_i}{\partial x_i} = \frac{\partial}{\partial x_i}\left(\rho D_n \frac{\partial Y_i}{\partial x_i}\right) + R(Y,T)S_n \tag{2.4}$$

Here i represents chemical species (i = 1,2,...,n), Y is chemical species vector, D_n is the is the species diffusivity. The chemical source term can be written in terms of the net rate formation of the species n. Generally, the assumption of Newtonian fluid where the shear stress are related through the dynamic viscosity, μ, and the strain rate is introduced. Thus, the viscous stress is described by equation (2.5).

$$\tau_{ij} = \mu\left(\frac{\partial u_i}{\partial x_j} + \frac{\partial u_j}{\partial x_i}\right) \tag{2.5}$$

2.2.2 Reacting Flows

To model reacting flow, two types of models including reacting species transport and flamelet are considered.

In reacting species transport models, the conservation equations which include the chemical source term are solved for all species in a mechanism. The reacting species transport modeling approach is suitable for reacting flow systems in which the mixing timescale is shorter than the reaction timescale for one or more species. This approach is useful for simulating slowly forming pollutants, part-load conditions in combustors, and transient combustion such as explosions, ignition, and extinction. However, the interaction between turbulence and chemical reactions adds another layer of complexity. Capturing these interactions accurately requires advanced turbulence models and can significantly increase computational requirements. Another drawback of this model is that detailed reaction mechanisms can involve hundreds of species and thousands of reactions, making the model complex and difficult to solve.

In flamelet models, the reacting flow system is simplified by using a small set of flamelet variables to describe the thermochemical conditions in each computational cell. Instead of solving equations for every species, only these flamelet variables are addressed[11]. Compared to the traditional approach of reacting species transport, the flamelet method significantly reduces computational costs by solving a smaller number of transport equations and pre-solving the chemistry of the reaction mechanism prior to the CFD simulation. The flamelet modeling approach is suitable for reacting flow systems in which the reaction timescale is shorter than the mixing timescale. This approach is particularly effective for steady-burning furnaces and burners, and full-load conditions in combustors. Nevertheless, flamelet models assume that the flame structure is thin compared to the turbulent scales. This assumption may not hold in all combustion regimes, particularly in highly turbulent or thickened flames.

In reacting flow simulations, the main difference between each of the reacting flow models is how the chemical source term is formulated to be used to solve continuity equation and the conservation equation. For reacting species transport models, the conservation equations for all species are solved using the mass fraction of the species. For flamelet models, the conservation equations are not solved for the species mass fractions. Instead, conservation equations are solved for the relevant flamelet variables including mean mixture fraction, fraction variance, unnormalized progress variable, unnormalized progress variable variance when using the Flamelet Generated Model (FGM) The chemical source term is also included in each progress variable conservation equation.

2.2.2.1 Reacting Species Transport

In StarCCM+, there are three models available for reactions species transport including Complex Chemistry, Eddy Break-Up and Eddy Contact Micromixing. In this study, Complex Chemistry is chosen since this model is suitable for introducing

detailed chemistry information. For complex chemistry, the general species transport equation is formulated as shown in equation (2.6)

$$\frac{\partial}{\partial t}\rho Y_i + \frac{\partial}{\partial x_j}\left(\rho u_j Y_i + F_{k,j}\right) = \omega_i \tag{2.6}$$

where Y_i is species mass fractions, $F_{k,j}$ is the diffusion flux component and source term ω_i is the rate of production of species i. The species transport equation is solved with an explicit reaction source term ω_i for species i given as equation (2.7)

$$\omega_i = \rho f \left(\frac{Y_i^* - Y_i}{\tau}\right) \tag{2.7}$$

where f is the mean reaction rate multiplier, τ is the time scale and Y_i^* is the mass fraction at the end of time integration. For the Laminar Flame Concept model (LFC), the mean reaction rate multiplier, *f,* is 1, and the time scale, τ, is the residence time in the cell.

The laminar flame concept model is a fundamental approach used to understand and describe combustion processes. However, it relies on several strong assumptions that can limit its applicability in more complex or turbulent combustion scenarios. The model assumes a one-dimensional flame structure, meaning that variations in properties occur only in the direction normal to the flame front, and it often assumes steady-state conditions where flame properties do not change with time. It also presumes a thin flame front compared to the characteristic length scales of the flow, allowing for a clear separation between the preheat zone, reaction zone, and post-flame zone. Additionally, the model typically assumes constant thermophysical properties, neglects radiative heat transfer, and uses simplified chemical reaction mechanisms. By definition, the laminar flame concept assumes a laminar flow regime, where the effects of turbulence are negligible with the assumptions of uniform initial conditions for temperature, pressure, and composition in the unburnt gas. The model often neglects diffusive transport effects and frequently assumes that the gas behaves as an ideal gas. While these assumptions simplify the analysis and provide valuable insights into the fundamental behavior of laminar flames, they limit the model's applicability to more complex, real-world combustion scenarios.

2.2.2.2 Flamelet Model

To reduce computational expense in combustion simulations, reactions for representative scenarios and tabulate the relevant quantities can be precomputed. A turbulent flame can be approximated as an ensemble of laminar flamelets. A flamelet refers to a fundamental 0D or 1D laminar flame shape. When flamelets are computed, the intricate thermo-chemistry involving temperature and species within the flame is represented by two or more variables. The Flamelet Generated Manifold (FGM) model assumes that the thermo-chemical conditions within a turbulent flame resemble those found in a laminar flame. These conditions are characterized by mixture fraction Z, reaction progress c, and enthalpy h. Since there is only one active reacting variable (the reaction progress, c), the model represents a single chemical time scale associated with heat release reactions.

2.2.2.2.1 Probability Density Function In modeling of reactive mixing a very important tool is probability density function (PDF) of a mixture fraction. The mixture fraction (ξ) is defined for binary mixtures as unity for one inlet stream and zero for the other. It describes how large a fraction of the flow at a certain point has historically come from the injection with a value of unity. A time series of concentrations can be obtained from measuring continuously at any small point.The histogram, or probability density, of raw data is defined as the probability of measuring a certain concentration of the tracer as shown in equation (2.8).

$$\varphi(\eta)d\eta \equiv Probability\ of\ \eta \leq \xi \leq \eta + d\eta \tag{2.8}$$

where η is a sample-space variable for ξ. A sample space is the collection of all possible outcomes of the event. A variable used to describe a single event in sample space is a sample-space variable. In mixture-fraction space η is thus the sample-space variable used to describe the real event ξ. The sample space of the mixture fraction spans from zero to unity, thus, the integral of the PDF must equal unity.

$$\int_0^1 \varphi(\eta)d\eta = 1 \tag{2.9}$$

The PDF indicates the fraction of time that the mixture fraction spends in the state, i.e. the fraction of time a certain concentration or mixture fraction is observed. The PDF contains all single-point information of the mixture fraction. Given the PDF, all mixture fraction moments (mean, variance, etc.) can be found by integration over mixture-fraction space. The mean $\langle\xi\rangle$ and variance σ^2 of the mixture fraction are defined through the PDF as shown in equation (2.10) and (2.11)

$$\langle\xi\rangle = \int_0^1 \varphi(\eta)d\eta \tag{2.10}$$

$$\sigma^2 = \int_0^1 (\eta - \langle\xi\rangle)^2\varphi(\eta)d\eta \tag{2.11}$$

During mixing, the variance is gradually decreased until eventually the mixture is homogeneous, the variance will be zero and the PDF can be described by a single Dirac delta-function. The beta-PDF uses the mean and variance of the mixture fraction to give a continuous distribution. The position of the peak is determined by the mean mixture fraction and the width by the variance.

In the flamelet generated manifold model (FGM), combustion is restricted to specific regimes where the PDF of the reaction progress variable and mixture fraction are assumed to be known. This method allows for the derivative of relationships for the mean reaction rate based on local quantities like flame surface density or scalar dissipation rate. The laminar reaction rate is tabulated based on laminar flame chemistry, with tables developed using key parameters. The reaction rate is then obtained from integration of the laminar reaction over presumed PDF for the key input values to the FGM table.

The mixture fraction is calculated as shown as

$$\xi = (\frac{m_f}{m_f + m_{ox}}) \tag{2.12}$$

where m_f is the total mass of all elements that originate from the fuel stream and m_{ox} is the total mass of all elements that originate from the oxidizer stream.
The transport equation for the mixture fraction when assuming unity Lewis number or equal species diffusivity is

$$\frac{\partial \rho \xi}{\partial t} + \frac{\partial \rho u_k \xi}{\partial x_k} = \frac{\partial}{\partial x_k}\left(\rho D_\xi \frac{\partial \xi}{\partial x_k}\right) \tag{2.13}$$

The progress variable c indicates whether the chemical state within a cell represents the unburnt conditions ($c = 0$), burnt conditions ($c = 1$), or something in-between ($0< c <1$). The reaction progress variable either monotonically decreases or increases across the flame and is typically defined based on temperature or certain major species. The unnormalized progress variable can be expressed as a weighted linear combination of species mass fractions, as illustrated in equation (2.14)

$$y = \sum(W_k Y_k) \tag{2.14}$$

where W_k is a weight function of specie k and Y_k is the mass fraction of the specie k. Many alternative combinations of species and weight factors have been suggested. However, for pure hydrogen combustion, the weight factor used to calculate the unnormalized progress variable is set to 1 for water because water formation is often the dominant reaction in hydrogen combustion. By setting the weight factor for water to 1, the unnormalized progress variable is effectively scaled to emphasize the importance of water formation in the overall combustion process. The progress variable is then defined as

$$c = \frac{y - y_u}{y_b - y_u} \tag{2.15}$$

Where y_u is the unnormalized progress variable at the unburnt state and y_b is the unnormalized progress variable at the burnt (equilibrium) state. The corresponding transport equations for the reaction progress is shown in equation (2.16)

$$\frac{\partial \rho c}{\partial t} + \frac{\partial \rho u_k c}{\partial x_k} = \frac{\partial}{\partial x_k}\left(\rho D_c \frac{\partial c}{\partial x_k}\right) + \rho \dot{\omega}_c \tag{2.16}$$

2.3 Modeling of Turbulence

The majority of fluid flows relevant to engineering is characterised by irregular fluctuations in flow properties. These fluctuations occur at small scales and high frequencies, making their prediction in both time and space impractical due to the substantial computational demands involved. Rather than directly solving the governing equations of turbulent flows through methods like Direct Numerical Simulation (DNS), it is more cost-effective to solve for averaged or filtered quantities, approximating the effects of small fluctuating structures. It is widely acknowledged

that all turbulence models are approximations of the actual turbulence phenomena. The level of approximation in a particular model depends on the characteristics of the flow. Evaluating the performance of a turbulence model largely relies on empirical experience and validation with experimental data. Turbulence models offer various approaches to model these structures. Turbulence can be categorized into two main categories which are Reynolds-Averaged Navier-Stokes (RANS) turbulence models and Scale-resolving simulations[10].

2.3.1 Reynolds-Averaged Navier-Strokes (RANS) models

To avoid, resolving all small scales, RANS models are used to close the system of equations in turbulent flows. They provide closure relations for the Reynolds-averaged quantities. These models assume that the flow variables can be decomposed into mean (time-averaged) and fluctuating components.

$$U_i = \langle U_i \rangle + u_i \tag{2.17}$$

This method is referred to as Reynolds decomposition, by time averaging over a reasonable time period (larger then turbulence time scale but smaller than mean flow timescale), the turbulent fluctuations are divided from the non turbulence quantities. The time derivative of the mean flow in the RANS equations accounts for variations at timescales larger than those of turbulence. The equations for the mean variables are derived by substituting the decomposed form into the Navier-Stokes and taking the average. Here the most interesting phenomena, momentum conservation, is considered and the general form of the RANS equation can be written as

$$\frac{\partial \langle U_i \rangle}{\partial t} + \langle U_j \rangle \frac{\partial \langle U_i \rangle}{\partial x_j} = -\frac{1}{\rho}\frac{\partial}{\partial x_j}\left(\langle P \rangle \delta_{ij} + \mu \left(\frac{\partial \langle U_i \rangle}{\partial x_j} + \frac{\partial \langle U_j \rangle}{\partial x_i} \right) - \rho \langle u_i u_j \rangle \right) \tag{2.18}$$

The term $-\rho\langle u_i u_j \rangle$ is Reynolds stress and it introduces a coupling between the men and fluctuating parts of the velocity field. Reynolds stress represents the average momentum flux due to the velocity fluctuations, thus characterizing the transfer of momentum by turbulence. The individual Reynolds stresses in the stress tensor, $\tau_{ij} = -\rho\langle u_i u_j \rangle$ are

$$\tau_{ij} = -\rho \begin{pmatrix} \langle u_1 u_1 \rangle & \langle u_1 u_2 \rangle & \langle u_1 u_3 \rangle \\ \langle u_2 u_1 \rangle & \langle u_2 u_2 \rangle & \langle u_2 u_3 \rangle \\ \langle u_3 u_1 \rangle & \langle u_3 u_2 \rangle & \langle u_3 u_3 \rangle \end{pmatrix} \tag{2.19}$$

Reynolds stresses is introduced to RANS equations without adding any extra equations and this means that it must be modeled. One way to model the Reynolds stress is to relate them to the dependent variables they are meant to transport. One straightforward approach involves expressing the Reynolds stress tensor using the mean velocity. However, this method is only an approximation, meaning that solutions obtained from RANS equations are always approximate. Subsequently, the closures that rely on the concept of turbulence eddy viscosity is explored.

2.3.1.1 Eddy Viscosity Models

The most common eddy viscosity model is known as Boussinesq approximation. It is based on the assumption that the components of the Reynolds stress tensor are proportional to the mean flow quantities. The Boussinesq relation proposes that the transport of momentum by turbulence is a diffusive process and that the Reynolds stresses can be modeled using a turbulent viscosity which is analogous to molecular viscosity. The Boussinesq approximation is written as equation (2.20)

$$\frac{\tau_{ij}}{\rho} = -\langle u_i u_j \rangle = \mu_t \left(\frac{\partial \langle U_i \rangle}{\partial x_j} + \frac{\partial \langle U_j \rangle}{\partial x_i} \right) - \frac{2}{3} k \delta_{ij} \tag{2.20}$$

where k is the turbulent kinetic energy per unit mass and is defined as half the trace of the Reynolds stress tensor, $k = 1/2\langle u_i u_i \rangle$. As part of quantitative turbulence modeling the eddy viscosity μ_t must be determined. For practical engineering purposes, the most successful models involve two additional transport equations. A straight forward approach to model the turbulent velocity and length scale is to solve the k equation for the velocity scale and the l equation for the length scale. The energy-dissipation rate, ε, and specific dissipation are the most commonly use to determine the kinetic energy and length scale.

Standard $k - \varepsilon$ model

The standard $k - \varepsilon$ turbulence model is one of the most widely used turbulence models in computational fluid dynamics. It is a two-equation model that aims to simulate turbulent flows by solving two additional transport equations for turbulent kinetic energy k and turbulent dissipation rate ε. The model assumes that the turbulence is isotropic and can be fully characterized by these two parameters. The turbulent kinetic energy represents the energy associated with turbulent fluctuations in velocity. The transport equation for k accounts for the production, diffusion, dissipation, and turbulent transport of kinetic energy. It is often modeled using a turbulent viscosity hypothesis, where the turbulent viscosity is related to k and the length scale. The turbulent dissipation rate represents the rate at which turbulent kinetic energy dissipates into internal energy due to viscous effects. The transport equation for ε describes how this dissipation rate changes throughout the flow field.

Lag Elliptic Blending $k - \varepsilon$ model

The Lag Elliptic Blending model combines the Standard Elliptic Blending model with the stress-strain lag concept and it helps to improve the stability of $k-\varepsilon$ model. The Elliptic Blending turbulence model solves two additional transport equations which are the normalized (reduced) wall-normal stress component φ, and the elliptic blending factor α in order to determine the turbulent eddy viscosity. In flow areas where non-equilibrium conditions cause a misalignment between the principal components of stress and strain-rate tensors, conventional linear eddy viscosity models often overestimate k production. To address this issue, the Lag Elliptic Blending model considers the angle between these components. It also introduces additional terms to account for anisotropic, curvature and rotational effects. These terms are

directly integrated into the transport equation for the reduced stress function φ [12]. The Lag Elliptic Blending model demonstrates strong predictive capabilities in scenarios involving separated or unsteady flow (such as vortex shedding) or when the flow experiences rotation or significant streamline curvature.

SST $k-\omega$ model

The SST (Shear Stress Transport) $k-\omega$ turbulence model is developed to apply especially for turbulent boundary layers, shear flows, and transitional flows. This model is the improvement of standard $k-\omega$ which incorporates equations for both the turbulent kinetic energy k and the specific rate of dissipation ω . The model employs ω near walls and in adverse pressure gradient regions to improve accuracy. SST model combines elements from both $k-\varepsilon$ and $k-\omega$ models [13]. Near solid boundaries, it applies $k-\omega$ model to accurately resolve near-wall turbulence, while in the bulk, it transitions to $k-\varepsilon$ model.

2.3.2 Large Eddy Simulation (LES)

Large Eddy Simulation (LES) is a sophisticated computational technique used in the field of fluid dynamics to simulate the turbulent flows of fluids. It is particularly useful in scenarios where understanding the behavior of large-scale eddies such as swirling patterns and their interaction with smaller scales is crucial. LES works by applying a spatial filter to the Navier-Stokes equations, This filtering process separates the large-scale motions from the smaller-scale motions. The large eddies, which contain most of the energy and are more influenced by boundary conditions and geometry, are directly resolved in the simulation. These are the primary carriers of momentum and energy in a turbulent flow. The effects of the smaller eddies are not directly computed but are modeled using a subgrid-scale model. This is necessary because fully resolving every scale of motion in a turbulent flow is computationally prohibitive with current technology. By resolving the larger scales of motion and modeling the smaller scales, LES can provide more accurate and detailed insights into turbulent flows compared to RANS and substantially save computational costs compared to DNS.

According to LES recommendations [10], the Kolmogorov length scale (η) and Taylor microscale (λ) are employed as the simplest filtering method to ensure that all large eddies are captured and small eddies are modeled effectively. These scales determine the appropriate cell size for LES simulations to model eddies down to the inertial range. Consequently, the suitable cell size (Δ) for further filtering in LES simulations is defined as $\eta < \Delta < \lambda$. These length scales are presented in equations (2.21) and (2.22).

$$\eta = (\frac{v^3}{\varepsilon^4})^{1/4} \tag{2.21}$$

$$\lambda = (\frac{10vk}{\varepsilon})^{1/2} \tag{2.22}$$

In contrast to the RANS equations, which are derived through an averaging process, the equations solved for LES are obtained via spatial filtering. By filtering the Narvier-Stokes equations, the scales which will be modeled are separated from those which will be calculated directly. Each solution variable ϕ is decomposed into a filtered value $\overline{\phi}$ (resolved by computational grid) and a subgrid value ϕ' (modelled).

$$\phi = \overline{\phi} + \phi' \tag{2.23}$$

$$U = \overline{U} + U' \tag{2.24}$$

The equations for the filtered quantities can be derived by incorporating the decomposed solution variables into the Navier-Stokes equations. The filtered continuity equation and the filtered momentum equation can be defined as equation (2.25) and equation (2.26), respectively.

$$\frac{\overline{U_i}}{\partial x_i} = 0 \tag{2.25}$$

$$\frac{\partial U_i}{\partial t} + \frac{\partial \overline{U_i}\,\overline{U_j}}{\partial x_j} = -\frac{1}{\rho}\frac{\partial \overline{p}}{\partial x_j} + \frac{\partial \overline{\tau_{ij}^{\nu}}}{\partial x_j} - \frac{\partial \tau_{ij}}{\partial x_j} \tag{2.26}$$

Here $\overline{U_i}$ denotes the filtered velocity. The filtered viscous stress, $\overline{\tau_{ij}^{\nu}}$, is given in term of the filtered velocity as

$$\overline{\tau_{ij}^{\nu}} = \nu\left(\frac{\partial \overline{U_i}}{\partial x_j} + \frac{\partial \overline{U_j}}{\partial x_i}\right) = 2\nu\overline{S_{ij}} \tag{2.27}$$

The strain rate tensor can be defined as

$$\overline{S_{ij}} = \frac{1}{2}\left(\frac{\partial \overline{U_i}}{\partial x_j} + \frac{\partial \overline{U_j}}{\partial x_i}\right) \tag{2.28}$$

2.3.2.1 Subgrid Stress Modeling

The subgrid scale turbulent viscosity (ν_t) is described by a subgrid scale model that accounts for the influences of small eddies on the resolved flow. In this study, the Wall-Adapting Local-Eddy (WALE) subgrid scale method is considered. WALE is designed to improve the representation of turbulence in LES by dynamically adapting the eddy viscosity based on the local flow characteristics near the wall. It aims to address shortcomings of traditional eddy-viscosity models, particularly in regions of high shear or near solid boundaries, where standard models may struggle to capture the correct turbulent behavior. The WALE model achieves this by incorporating a length scale that adapts to the local flow features, particularly near the walls, where turbulence is strongly influenced by the presence of solid boundaries. This adaptation helps to better model the anisotropic nature of near-wall turbulence, improving the accuracy of LES simulations, especially in flows with complex geometries or near solid surfaces. The subgrid scale turbulent viscosity (ν_t) is provided in equation (2.29) as a mixing-length type formula

$$\nu_t = \rho\Delta^2 S_w \tag{2.29}$$

where Δ represents the length scale or grid filter width and S_w represents a deformation parameter which can be calculated by equation (2.30)

$$S_w = \frac{S_d^{3/2}}{S_d^{5/4} + S_d^{5/2}} \tag{2.30}$$

The tensor S_d is defined as equation (2.31)

$$S_d = \frac{1}{2}[(\nabla v \cdot \nabla v)^T] - \frac{1}{3} tr(\nabla v \cdot \nabla v)\mathbf{I} \tag{2.31}$$

Where I is an identity tensor

2.3.2.2 Evaluation of LES Resolution

As a general rule of thumb, at least 80% of the turbulent kinetic energy should be resolved by the filtered velocity field and this is known as Pope criterion. This corresponds to the ratio of resolved turbulent kinetic energy (k_{res}) to the overall turbulent kinetic energy ($k_{res} + k_{SGS}$).If this ratio equals to one, it corresponds to DNS and indicates that the flow is very well resolved. If this ratio equals to zero, it indicates poor resolution of LES.

$$\frac{k_{res}}{k_{res} + k_{SGS}} > 0.8 \tag{2.32}$$

Here, k_{res} and k_{SGS} can be calculated from Equation (2.33) and Equation (2.34), respectively.

$$k_{res} = \frac{1}{2}(v_{i,RMS}^2 + v_{j,RMS}^2 + v_{k,RMS}^2) \tag{2.33}$$

$$k_{SGS} = \frac{C_t \mu_t S}{\rho} \tag{2.34}$$

where C_t is 3.5 and the RMS values can be obtained from the square root of field variance data.

2.4 Chemical Mechanism

For accurate simulation of hydrogen combustion, a detailed chemical kinetic mechanism is required that encompasses all relevant reactions and species involved in the process. Hydrogen has a relatively simple combustion mechanism compared to hydrocarbons like methane. This is because it consists mainly of reactions involving H_2, O_2, and their intermediates such as OH, H, O, and HO_2.The rates of reactions in hydrogen combustion are highly dependent on temperature and pressure, which must be accurately modeled for realistic simulation outcomes. The choice of mechanism often depends on the specific application and the required accuracy versus computational resource constraints. As hydrogen technology continues to develop, these models are continually refined and expanded to better match experimental observations and practical needs. However, there are three mechanisms to be studied in this thesis which are GRI, FOI, and NUIG.

2.4.1 GRI Mechanism

GRI-Mech, is a widely recognized chemical kinetic mechanism developed primarily for modeling the combustion of natural gas including NO formation and reburn chemistry. It was developed by the Gas Research Institute. The mechanism contains 325 reactions and 53 species. The mechanism includes a wide range of reactive species such as radicals (e.g., OH, HO_2, CH_3), stable molecules (e.g., CO_2, H_2O), and intermediate hydrocarbons. Several testing of GRI mechanism against experimental data such as ignition delays and laminar flame speeds have been conducted The details of the reaction mechanism, rate coefficient, thermodynamical data and parameters needed for calculating transport coefficients can be accessed. While GRI mechanism is comprehensive, it has some limitations. The large number of reactions and species can make simulations computationally intensive. Besides, it is primarily tailored for natural gas combustion and might need modifications for other fuels, in this case hydrogen [14] [15].

2.4.2 FOI Mechanism

FOI or Z24 mechanism is a detailed chemical kinetic model specifically designed for simulating hydrogen-air combustion and developed by Swedish Defence Research Agency. It is developed to accurately capture the complex chemistry involved in hydrogen combustion processes, including ignition, flame propagation, product and pollutant formation. This mechanism contains 9 species and 24 irreversible reactions. The mechanism involves a multitude of chemical species relevant to hydrogen combustion, including reactants (H_2, O_2, N_2), intermediates (H, OH, HO_2), products (H_2O, NO, NO_2), and radicals (e.g., H, O, N) [16].

2.4.3 NUIG Mechanism

The NUIG (National University of Ireland, Galway) mechanism, specifically developed for hydrogen combustion, is a detailed chemical kinetic model that includes a set of reactions, species, and rate constants to accurately represent the combustion process of hydrogen. The primary reaction pathways and species are similar to FOI mechanism with minor modifications of the species and reactions involving NO formation [17].

3

Methodology

This chapter consists of the overall thesis methodology to set up the model for hydrogen combustion in StarCCM+ employing different chemical mechanisms, turbulence and combustion models.

3.1 Simulation Cases

In this thesis, different chemical mechanisms, turbulence models, and combustion models are evaluated to see the influence of each factor on the flame characteristics of pure hydrogen combustion. The chemical mechanisms used are GRI, FOI, and NUIG. Three RANS turbulence models are employed including LagEB $k-\varepsilon$, Standard $k-\varepsilon$, SST $k-\omega$. Then, they are further simulated using LES. Two different combustion models are applied consisting of Flamelet Generated Manifold (FGM) and Laminar Flame Concept (LFC). However, GRI mechanism is not applicable for LFC model since a numerous number of transport equation is required which is computational intense. A summary of the cases can be seen in Table 3.1.

3.2 Domain Set Up

In CFD simulation, the initial step involves creating a computational domain. StarCCM+, is used to solve the transport equations of mass, momentum and energy. The main steps include geometry and mesh generation, pre-processing, solver and post-processing.

3.2.1 Geometry

The burner geometry has been developed applying the micromix concept which potentially stabilizes the micro diffusion flames of pure hydrogen. The injectors have been tested in the Atmospheric Combustion Rig at the National Research Council Canada[18]. The single nozzle equipped with additive manufactured micromix injectors positioned in a cross pattern, the dimension of the burner is shown in Figure 3.1.

Table 3.1: Simulation cases.

case	Turbulence model	Mechanism	Combustion model
1	LagEB $k-\varepsilon$	GRI	FGM
2	LagEB $k-\varepsilon$	FOID	FGM
3	LagEB $k-\varepsilon$	NUIG	FGM
4	Standard $k-\varepsilon$	GRI	FGM
5	Standard $k-\varepsilon$	FOID	FGM
6	Standard $k-\varepsilon$	NUIG	FGM
7	SST $k-\omega$	GRI	FGM
8	SST $k-\omega$	FOID	FGM
9	SST $k-\omega$	NUIG	FGM
10	LES	GRI	FGM
11	LES	FOID	FGM
12	LES	NUIG	FGM
13	LagEB $k-\varepsilon$	FOID	LFC
14	LagEB $k-\varepsilon$	NUIG	LFC
15	LES	FOID	LFC
16	LES	NUIG	LFC

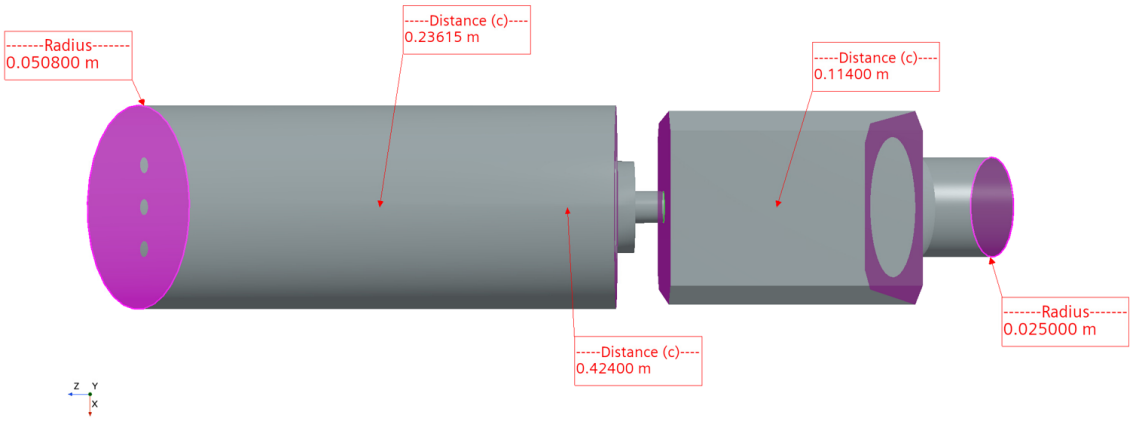

Figure 3.1: Overview of geometry and dimension of the burner.

The detailed configuration of the burner is indicated in Figure 3.2 where the air and hydrogen are fed separately at the inlet. The fuel is injected before the entrance of the chamber. The fuel is injected through these multiple holes to create small jets-in-cross flow, then mixed with air and burnt inside the combustion chamber. This burner is an academic set-up and has been developed to utilize micromix concept, that is able to stabilize premixed, partially premixed, and micromix flames of various fuel mixtures ranging from pure methane to pure hydrogen. Therefore, there is a pathway to feed methane into the system, but very insignificant amount of air is introduced instead for this study as only hydrogen is used as a fuel.

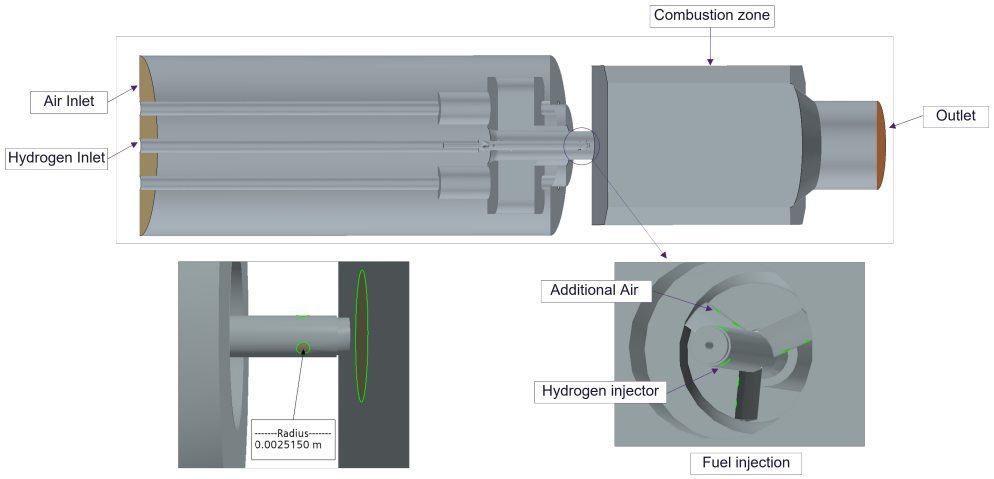

Figure 3.2: Cut section of the geometry with air and fuel inlets, injection, combustion zone and outlet.

3.2.2 Mesh Generation

The polyhedral meshes with a prism layer is applied to generate the mesh with the base size of 1 mm, the crucial parameters to construct the mesh are shown in Table 3.2. The mesh is refined according to the specific local surface cell sizes in all areas of interest. The starting point for this case is to have the cell size of 0.125 mm in fuel where injection takes place, 0.25 mm in the combustion chamber where the mixing and flame develop and 0.5 mm on the surface close to the fuel and air mixing. From this set up and refinement, the number of cell becomes 11.7 million cells. The mesh is then further refined at the most crucial points which are the area around fuel injection and mixing as shown in Figure 3.3. The cell size of the injection area is refined to become 0.1 mm and the jet-cross flow of Hydrogen is adapted to be 0.05 mm. The mixing zone is divided into two main parts, the first part is refined to be 0.2 mm to capture more detail of the mixing occurred and further expand to be 0.25 mm in the second part. After the second refinement, the number of cell becomes 21.1 million cells.

Table 3.2: Crucial parameters used for mesh set-up.

Parameter	**Value**
Base Size	1.0 mm
Surface Growth Rate	1.3
Prism Layer Total Thickness	0.33 mm
Volume Growth Rate	1.2 mm

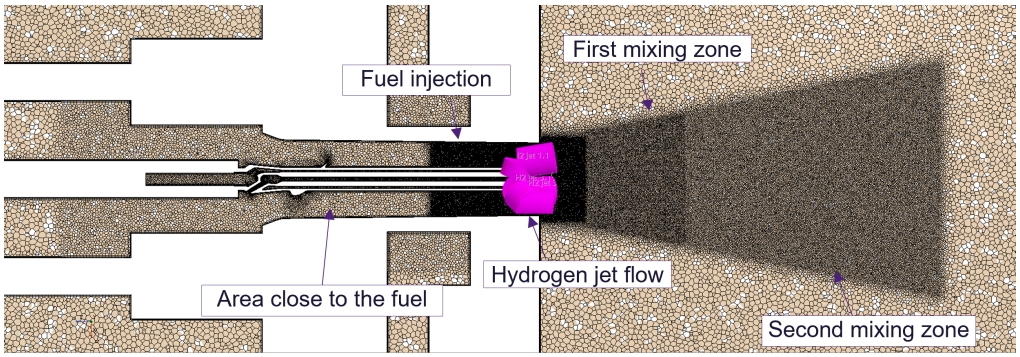

Figure 3.3: Overview of computational grid with the highlight of the area of interest.

3.2.3 Mesh Sensitivity

To validate the mesh, it is further refined to assure the mesh-independent results. The most critical critical area that affects the calculation is the area around the air-fuel jet cross flow. The meshes at this area are refined to be 0.03 mm and the number of cells becomes 39.2 million cells in total. The Taylor microscale is evaluated to be 0.02 mm at the area of the jet, this scale is tested and applied around the jet. It results 98 million cell mesh which is going to be very computationally intense. Therefore, the results from 21.1 million cell and 39.2 million cell cases are compared and validated.

3.2.4 Boundary Conditions

The mass flow inlet of fuel and air is defined and calculated such that the equivalence ratio becomes 0.615 because the flame temperature around 1858 K can be expected. The minimum of carbon monoxide (CO) and nitrogen oxide (NOx) can be reached around this temperature as shown in Figure 3.4. The inlet conditions of both air and fuel are provided in Table 3.3.

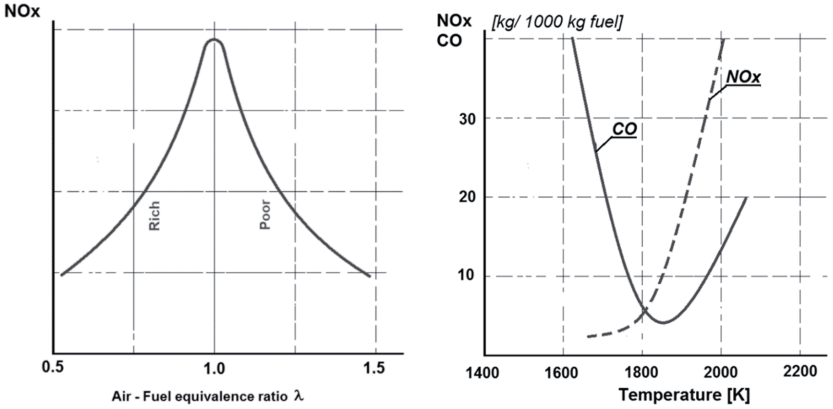

Figure 3.4: Influence of equivalence ratio on NOx emission and influence of combustion temperature on CO and NOx emission[19].

The Reynolds number (Re), turbulent intensity and turbulent length scale are calculated from equations (3.1), (3.2), and (3.3), respectively.

$$Re = \frac{\rho v L}{\mu} \tag{3.1}$$

$$I = 0.16 Re^{-1/8} \tag{3.2}$$

$$l = 0.07 L \tag{3.3}$$

Where ρ is the density, v is the velocity, L is the characteristic length and μ is the dynamic viscosity.

Table 3.3: Boundary Conditions.

Stream	**Parameter**	**Value**
Air Inlet	Mass flow inlet	13.7 g/s
	Bulk velocity	68.19 m/s
	Reynolds Number	1.45×10^5
	Turbulent Intensity	0.036
	Turbulent Length Scale	7 mm
Hydrogen Inlet	Mass flow inlet	0.24 g/s
	Bulk velocity	805.91 m/s
	Reynolds Number	5.65×10^4
	Turbulent Intensity	0.041
	Turbulent Length Scale	0.2 mm

3.3 Turbulence Modeling

3.3.1 Model Formulation

The selected models are shown in Table 3.4 and default values from StarCCM+ are used for any parameters which are not shown here.

Table 3.4: Physics continuum models.

Parameter	**Enable model**
Space	Three-dimensional
Time	Steady for RANS Implicit unsteady for LES
Components	Air and Hydrogen
Reacting Regime	Reacting
Viscous Regime	Turbulent
Flow	Segregated flow
Enthalpy	Segregated fluid enthalpy
Equation of state	Compressible ideal gas
Turbulence model	LagEB $k-\varepsilon$ Standard $k-\varepsilon$ SST $k-\omega$ LES
Subgrid scale turbulence (for LES)	WALE subgrid scale
Reacting flow model	Flamelet Reacting Species Transport
Flamelet model	Flamelet Generated model (FGM) FGM kinetic rate
Reacting Species Models	Complex Chemistry Laminar Flame Concept (LFC)
Wall treatment	All y+ wall treatment

Regarding model set-up, three-dimensional model is applied and time depends on the turbulence models. The flow is assumed to be segregated. The equation of state is considered to be a compressible ideal gas since a reasonably high Mach Number flow occurs around the jet area. According to material properties, the molecular diffusivity employs different methods for different reacting flow models. For the flamelete model, one general value of turbulent Schmidt number which is defined as the ratio between turbulent viscosity and turbulent diffusivity is applied to describe turbulent mixing. The general approach used a value of 0.9 for typical cases. For the reacting species transport model, different values are used for each component depending on its properties. Wall-Adapting Local Eddy-viscosity (WALE) is included to model subgrid scales in LES since it offers an improved representation of subgrid dissipation by considering both strain rate and rotational rate. In order to achieve low numerical diffusion, second order upwind scheme is used for convection and temporal discretization.

3.3.2 Transient Simulation

3.3.2.1 Initialization and Time Step

The use of transient simulations, especially LES turbulence models has been increasing in the industrial application due to its ability to capture dynamic behaviors and higher accuracy prediction than RANS. However, it comes with relatively high additional computational cost, thus, the simulation set-up needs to be treated properly.

For initialization, to accelerate the LES simulation, RANS modeling with steady condition is initially conducted and monitored until it converges. Then, it is further used as an initial condition for LES.

In order to ensure that the dynamics are captured accurately, the time step used for unsteady simulation is crucial. The time step is determined according to the Convective Courant-Friedrichs-Lewy number (CFL)[20] and it can be calculated by equation (3.4)

$$CFL = \frac{U\Delta t}{\Delta x} \tag{3.4}$$

where U is velocity scale, Δt is time step size and Δx is cell size. The time step used in the simulation should be less than the time at which flow properties travel from one cell to the neighbor cell. Therefore, CFL number ought to be lower than or equal to one. However, the velocity around the jet trajectory is significantly higher than the global value and this requires to very small time step to achieve CFL number of 1, hence, a slightly higher CFL number is accepted to essentially to obtain a balance between accuracy and computational efficiency. This criterion is accomplished by utilizing a time step of 1e-6 s.

3.3.2.2 Mean Field and Data Sampling

Creating a mean field of the data of interest is important when performing LES and it can be obtained using field mean monitors. The region to be sampled and the starting time should be carefully defined. The sampling frequency for field mean is usually set to 1 and the starting point should be selected so that the turbulence is fully developed, and any initial fluctuations have been excluded. In this study, the starting time to collect the data samples is determined by the number of flow-through times which is the time for a fluid particle to pass through the whole domain. According to the geometry and velocity, the fluid element has approximated 0.08 s of flow-through time. The simulations are running for 3-4 flow-through times before data averaging is initiated

3.4 Combustion Modeling

3.4.1 FGM Model

The mechanism files consisting of chemical kinetics, thermodynamics and transport files are imported to create the FGM table. The table is created by identifying the mass fraction of oxidizer and fuel to be air and hydrogen, respectively. The reactor type is selected to be 1D premixed strained. Absolute pressure is set to be 1.03 bar. The main species are chosen to be tabulated are H, H_2, H_2O, N_2, O_2, OH. It is important to define a proper number of grid points for each parameter as shown in Table 3.5 In the boundaries section, the fuel and air are defined by mixture fraction as 0 for and 1 for the fuel inlet. The exit is assigned with the conditions upstream for the case that recirculation may occur.

Table 3.5: Table dimensions for FGM model.

Parameter	Maximum number of grid points
Heat Loss Ratio	21
Mixture Fraction	101
Mixture Fraction Variance	11
Progress Variable	101
Progress Variable Variance	11

3.4.2 LFC Model

The mechanism files are imported under complex chemistry and chemistry acceleration is turned off to prevent avoid inaccurate calculations. For material property, the method to define dynamic viscosity is Mathur-Saxena averaging and individual values of molecular diffusivity are specified for each component.

4

Results and Discussions

The simulation results of pure hydrogen combustion in a micromix combustor using different turbulence models, chemical mechanisms, combustion models and the comparison between simulation and experimental results are summarized in this chapter.

4.1 Mesh Validation

Mesh validation is conducted to ensure that the results are independent of the mesh size [21]. The cases of 21.1 and 39.2 million cells are simulated using RANS and FGM model with GRI mechanism at the same boundary conditions. The field of temperature along the cutting plane and velocity at the mixing plane are compared and shown in Figure 4.1.

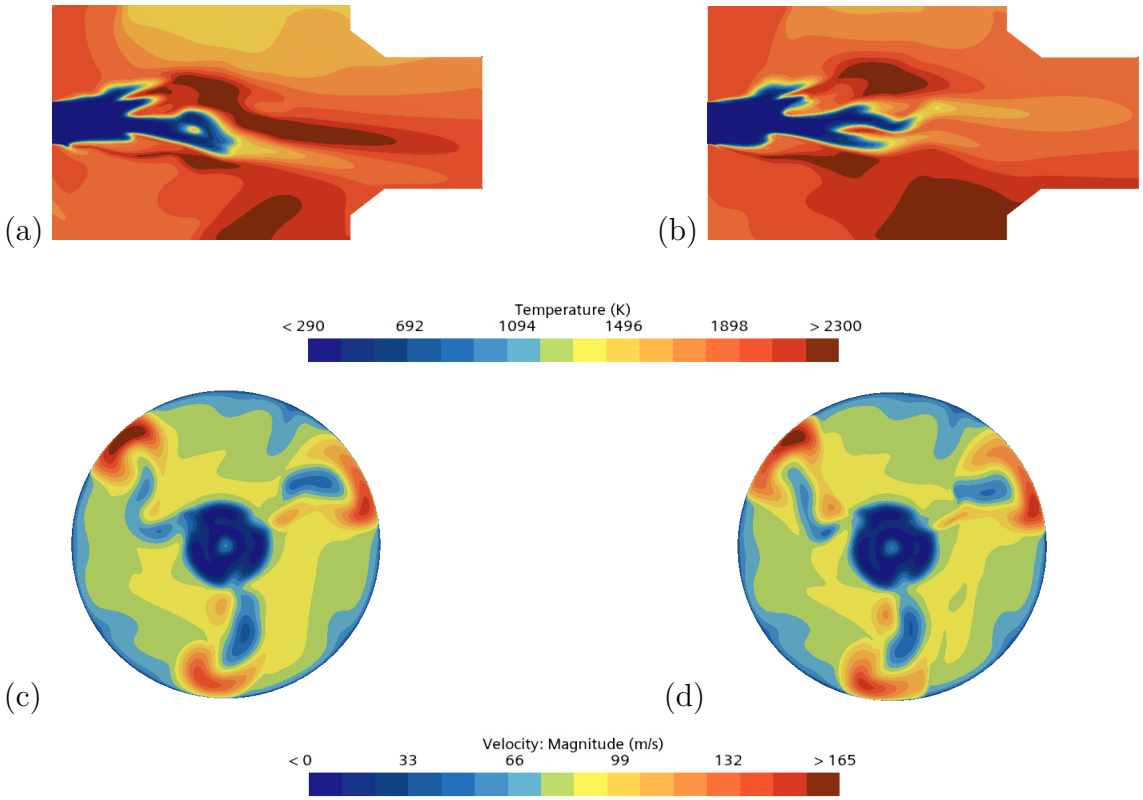

Figure 4.1: Temperature field at the cutting plane with 20 million cells (a) and 40 million cells (b). Velocity at the mixing plane with 20 million cells (c) and 40 million cells (d)

The field of mixture fraction at the mixing plane and progress variable along the cutting plane are compared in Figure 4.2.

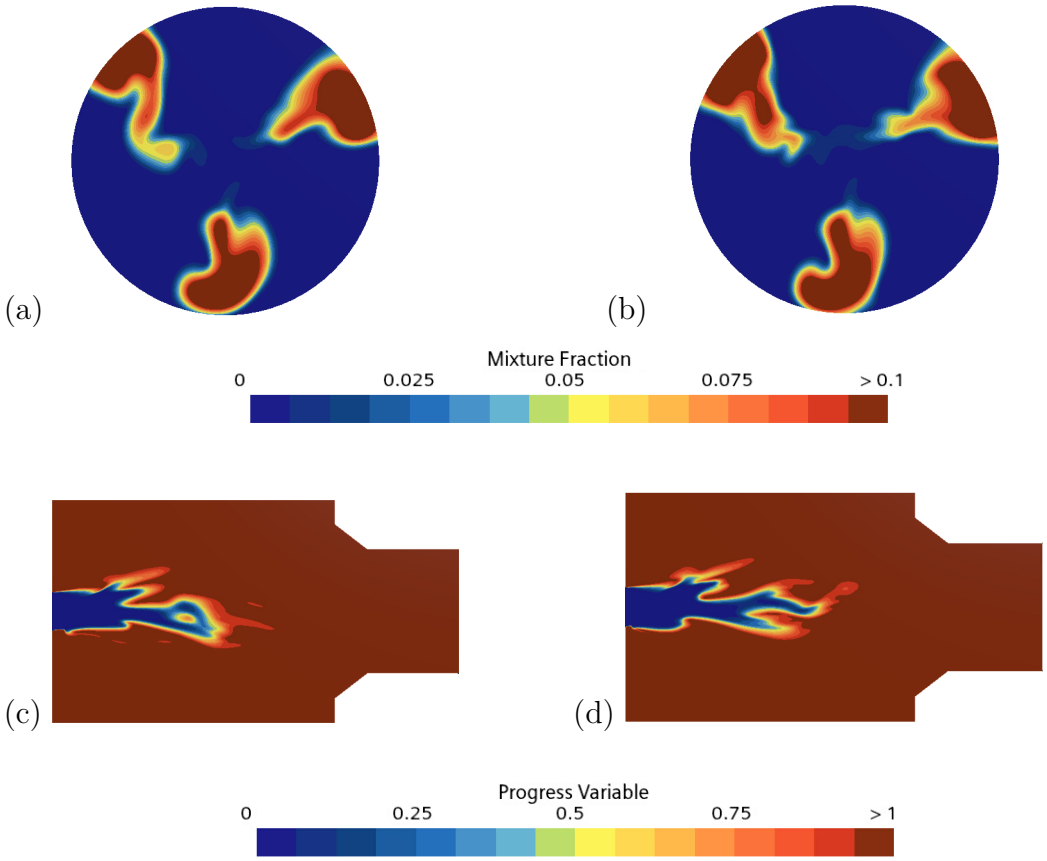

Figure 4.2: Mixture fraction at mixing plane with mesh of 20 million cells (a) and 40 million cells (b). Progress variable at cutting plane with 20 million cells (c) and 40 million cells (d)

It can be seen that the results are fairly similar between these two meshes. The mesh size around the hydrogen jet of 39.2 million cells is almost able to capture turbulent features related to the Taylor micro scale. This helps to improve accuracy but drastically increases computational cost. The insignificant changes of the results obtained from using double cell numbers makes it not worth the huge additional cost.

However, the asymmetry of the flow field should be noticed. The geometry consists of three small holes with identical diameters to inject hydrogen, hence the symmetric flow field at the mixing plane is expected. This asymmetry is further investigated to confirm the convergence by capturing the dynamics using unsteady RANS [22]. According to Figure 4.3, the velocity and mixture fraction at the mixing plane converged with asymmetry fields. Therefore, the asymmetry is the result of geometry and flow that may arise from the turbulence when the hydrogen jet is mixed with an air inlet.

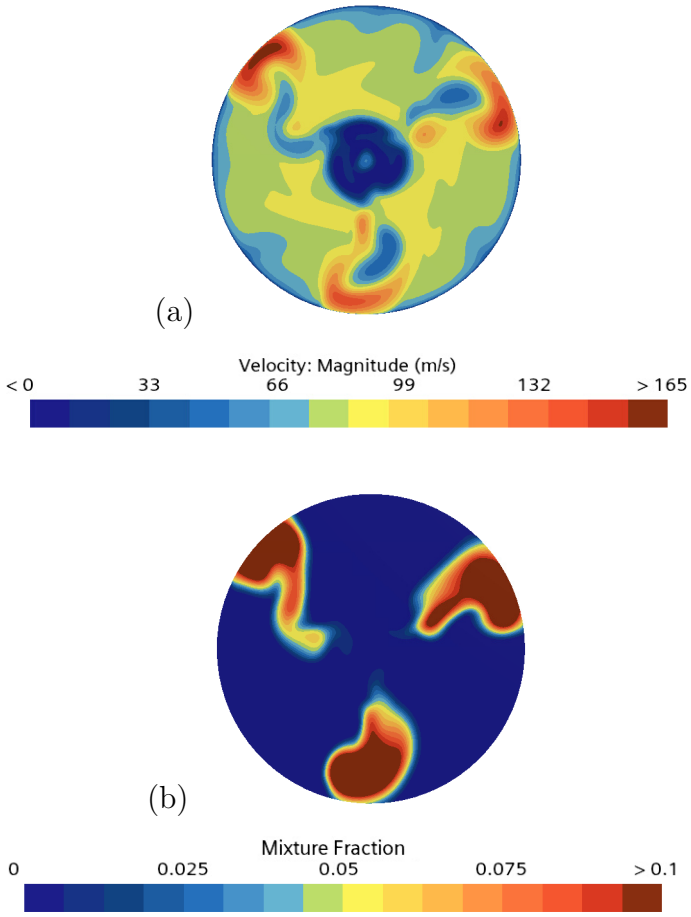

Figure 4.3: Velocity (a) and mixture fraction (b) field at the mixing plane from URANS of 20 million cell mesh.

4.2 Investigation of RANS Turbulence Models

Three RANS turbulence models are investigated including LagEB $k-\varepsilon$, standard $k-\varepsilon$, and SST $k-\omega$. The results in this section are obtained by using the GRI mechanism and FGM method. The temperature is predicted to be much lower than that from LagEB $k-\varepsilon$ as shown in Figure 4.4. The hydrogen mass fraction at the exit is higher in standard k-epsilon which is 5.32 μg compared to LagEB $k-\varepsilon$ which is 1.12 μg and it means that less hydrogen is reacted and burnt. The temperature field obtained from standard $k-\varepsilon$ shows an unusual flame front as can be seen in Figure 4.5. For the flow field and mixture fraction illustrated in Figures 4.6 and 4.7, the symmetric fields are obtained. Standard $k-\varepsilon$ fails to capture complex anisotropy that may occur near walls and it is limited to round jets and flows involving in significant curvature. Therefore, the swirl and asymmetric results are obtained in Figure 4.8. It shows the field of progress variable and it supports the fact that mixing occurred faster in LagEB $k-\varepsilon$ resulting in a more compact flame [23].

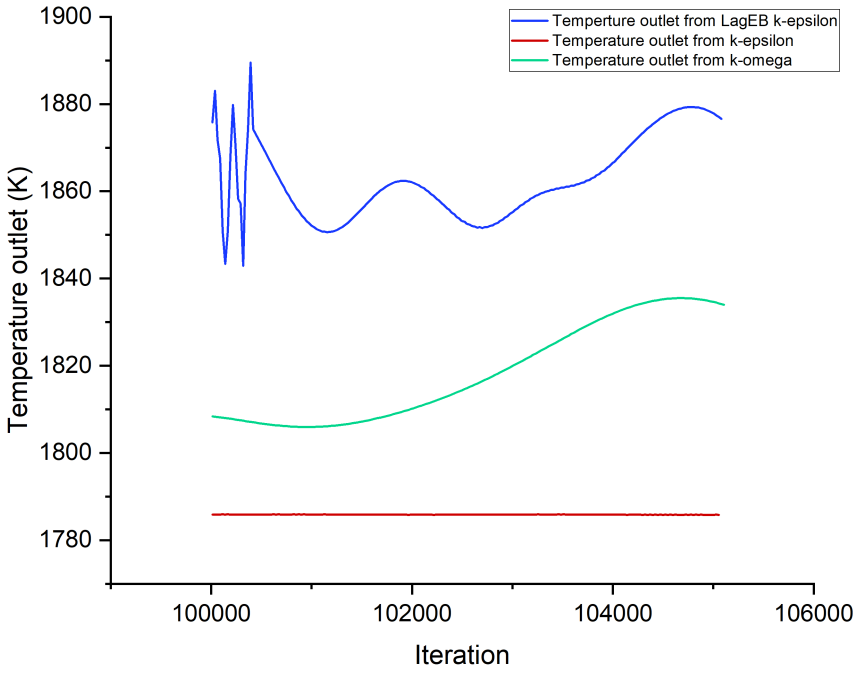

Figure 4.4: Comparison of the exit temperature between LagEB $k-\varepsilon$ (blue), standard $k-\varepsilon$ (red), SST $k-\omega$ (green).

For $k-\omega$, the difficulty to reach convergence is remarkable,and characterized by a huge fluctuation of the temperature in the range of 300 K. This may occur because of the need for fine mesh close to the wall which is not the main focus area (to refine the mesh) in this work, and this turbulence model may not be suitable for the flow conditions or geometry, alternatively the transient effects or highly unsteady flow behavior can hinder convergence from using this model. To further improve convergence, under-relaxation factors are decreased to 0.5 and an improvement can be observed, the exit temperature is more stable, but still lower than the adiabatic temperature. However, it will require a significant amount of time to reach convergence, hence, $k-\omega$ is not further discussed in the upcoming section.
Considering these three models, LagEB $k-\varepsilon$ is able to predict accurate flame temperature, close to that obtained from a calculation from adiabatic flame temperature which at this equivalence ratio is around 1858 K. This model is therefore used as basis in the other sections.

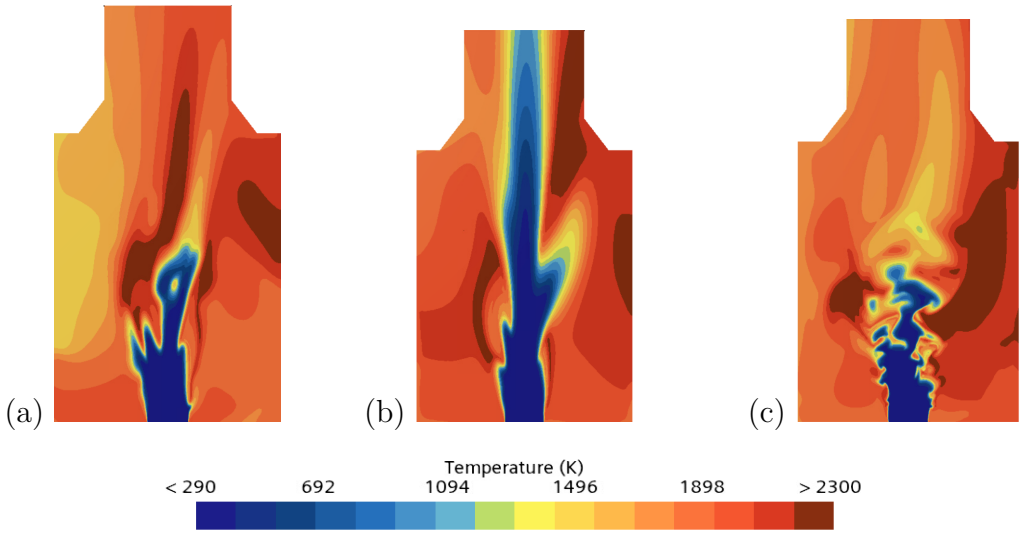

Figure 4.5: Temperature LagEB $k-\varepsilon$ (a), standard $k-\varepsilon$ (b), SST $k-\omega$ (c).

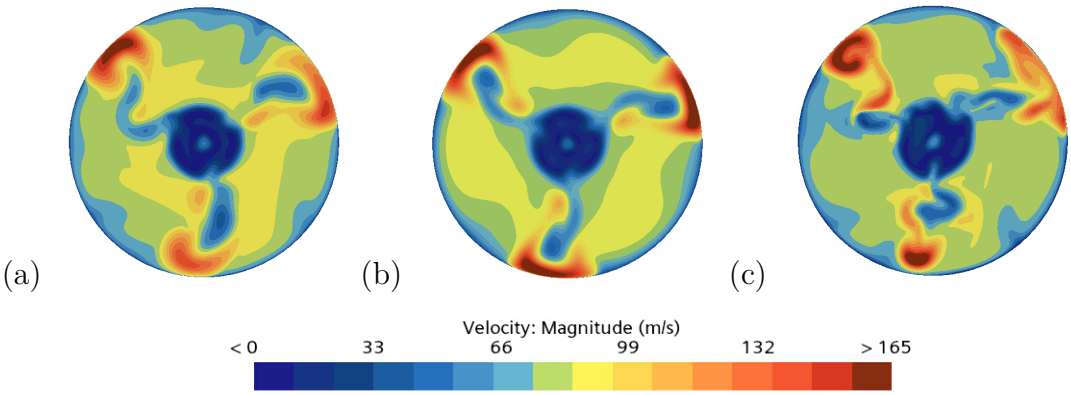

Figure 4.6: Velocity LagEB $k-\varepsilon$ (a), standard $k-\varepsilon$ (b), SST $k-\omega$ (c).

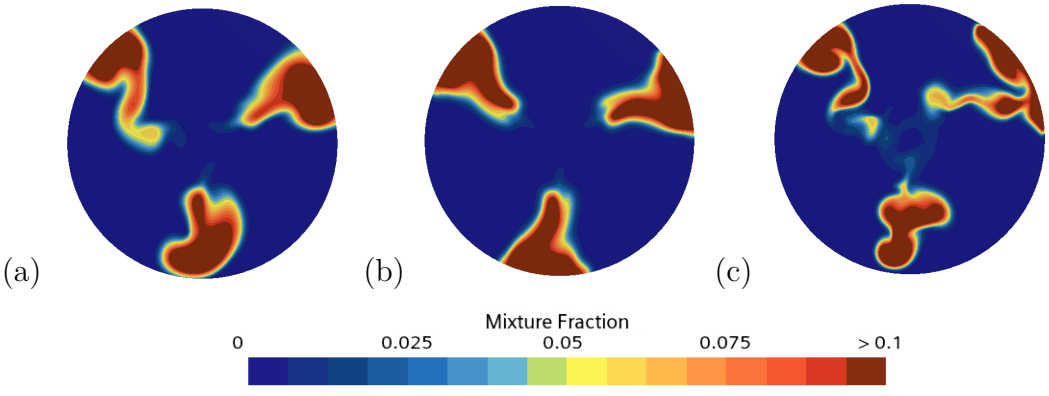

Figure 4.7: Mixture fraction LagEB $k-\varepsilon$ (a), standard $k-\varepsilon$ (b), SST $k-\omega$ (c).

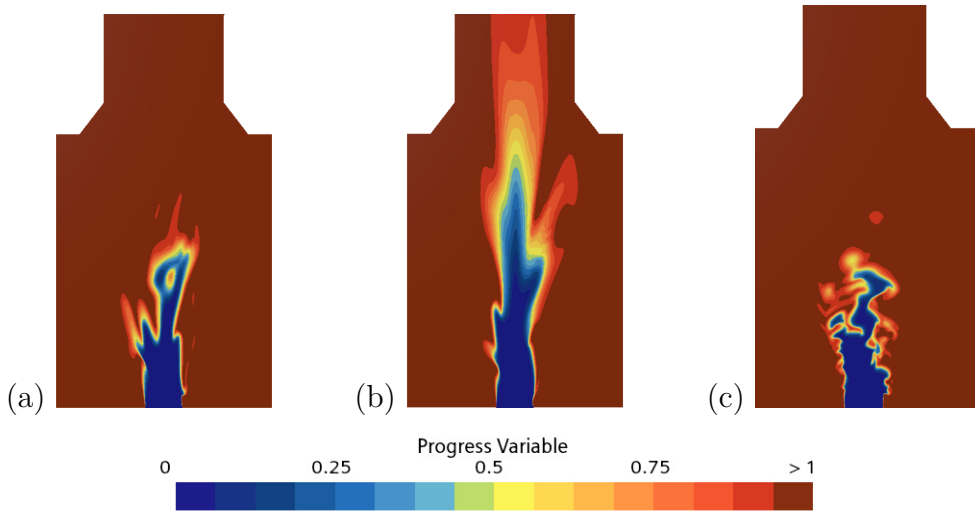

Figure 4.8: Progress variable LagEB $k-\varepsilon$ (a), standard $k-\varepsilon$ (b), SST $k-\omega$ (c).

4.3 Investigation of Chemical Mechanisms

The results when applying LagEB $k-\varepsilon$ and FGM model with different chemical mechanisms namely GRI, FOI and NUIG described in the methodology section are examined. Figures 4.9 and 4.10 show the field of temperature at the cutting plane and the temperature at the exit, respectively. The results from these three mechanism are fairly similar. The flame shapes are very much alike with the same range of temperature at the exit around 1850 - 1890 K. These three mechanisms likely incorporate similar reactive species, reaction pathways and rate expressions for hydrogen combustion. In addition, these mechanisms have been extensively validated against a broad range of experimental data, demonstrating their accuracy in reproducing key combustion phenomena at atmospheric condition. This consistency ensures that they produce comparable results. Nevertheless, the temperature at the exit fluctuates slightly above the adiabatic temperature (1858 K). This is a common drawback of simplified chemical descriptions based on steady-state assumptions. They often overestimate equilibrium temperatures because the enthalpy of formation of the steady-state species is not adequately considered in the energy balance, leading to an overprediction of heat release [24]. Due to this similarity, FOI mechanism is preferable and further applied to compare in the next section since it contains the least number of species. The number of species and reactions are, indeed, a major contributor to the expense of chemistry integration within a reactive flow simulation.

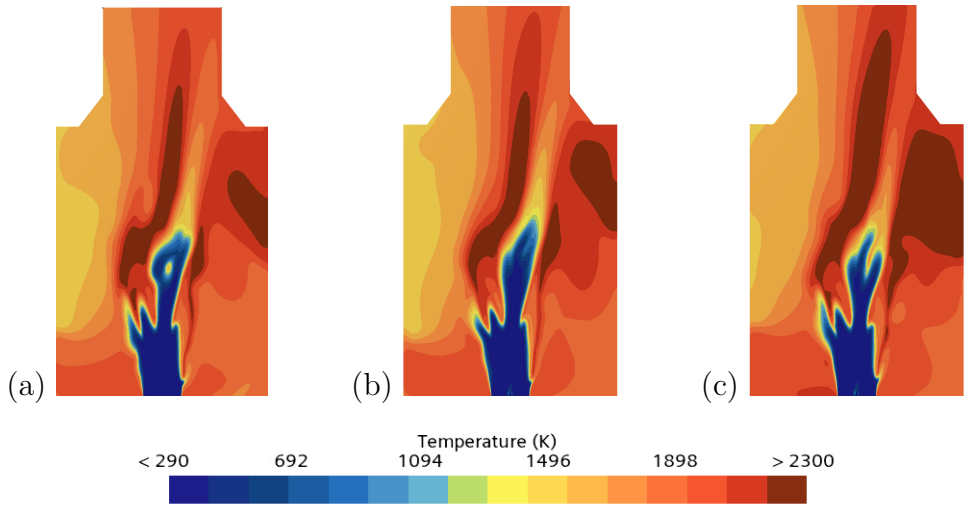

Figure 4.9: Temperature field from GRI (a), FOI (b), NUIG (c) mechanism.

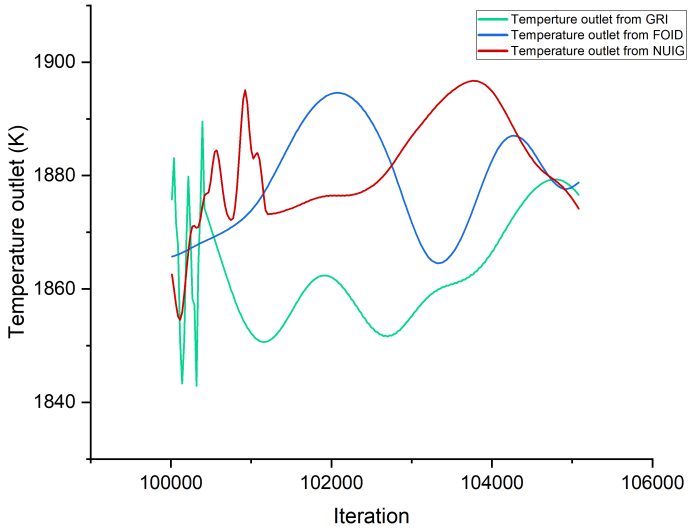

Figure 4.10: Comparison of the exit temperature for GRI (green), FOI (blue), and NUIG (red) mechanism.

4.4 Comparison between RANS and LES results

The results of implementing RANS LagEB $k-\varepsilon$ and LES with the same combustion model, FGM, and mechanism, FOI, are explored. Figure 4.11 shows the comparison between flame temperature and it is noticeable that hot spots are developed from RANS models. There are different factors that may cause hot spots to be pronounced in RANS. In regions where turbulent transport is significant, such as near walls or in regions of high shear, RANS models may not accurately predict the transport of heat and species, leading to erroneous predictions of temperature and concentration gradients and the formation of hot spots. Moreover, RANS models

often underestimate the dissipation of turbulent kinetic energy, especially in regions of high turbulence intensity or rapid flow acceleration or deceleration. This can result in an insufficient dissipation of kinetic energy, leading to the formation of local regions with elevated turbulence levels and increased temperature, i.e., hot spots. Another reason can be an inadequate grid resolution since the hot spots occur at the location where the cell sizes are compromised to reduce the computational cost. If the grid is not sufficiently fine to resolve small-scale turbulent structures, the model may not accurately capture the turbulent mixing processes that help dissipate heat and species concentrations, leading to the formation of localized regions with elevated temperature.

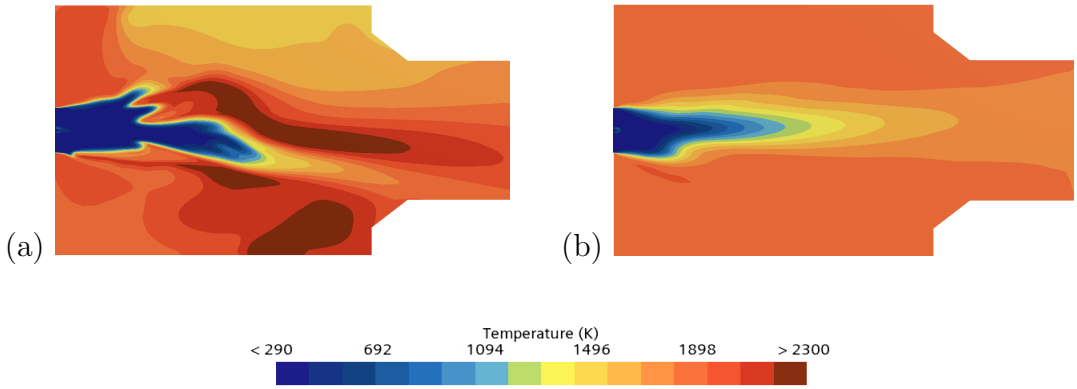

Figure 4.11: Comparison of temperature fields obtained from RANS (a) and LES (b).

Figure 4.12 shows the comparison between the exit temperatures from RANS and LES. The value are found to fluctuate a nd h igher i n R ANS a nd t his c an b e the result of hot spot formation and dynamics as discussed previously.

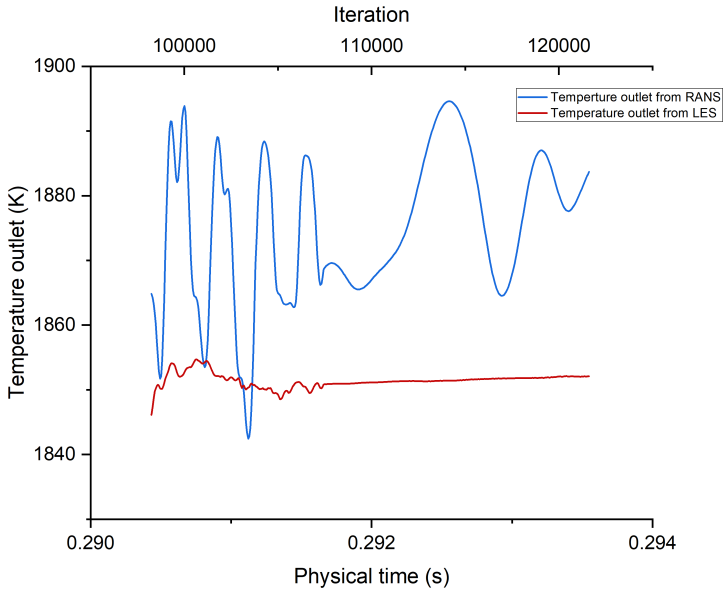

Figure 4.12: Comparison of exit temperature between RANS (blue) and LES (red).

LES resolution is evaluated by applying the Pope criterion [25] which suggests that the majority or more than 80% of the turbulent kinetic energy dissipation should be resolved by the grid (through resolved scales) rather than modeled by the subgrid scale model. In this study, 96% of the turbulent kinetic energy is resolved which can be seen in Figure 4.13. The critical area such as fuel injection and mixing are ensured to achieve the criterion, however, in the areas outside of the main focus the grid size may not be sufficient to reach the criterion, but acceptable to balance with simulation expenses.

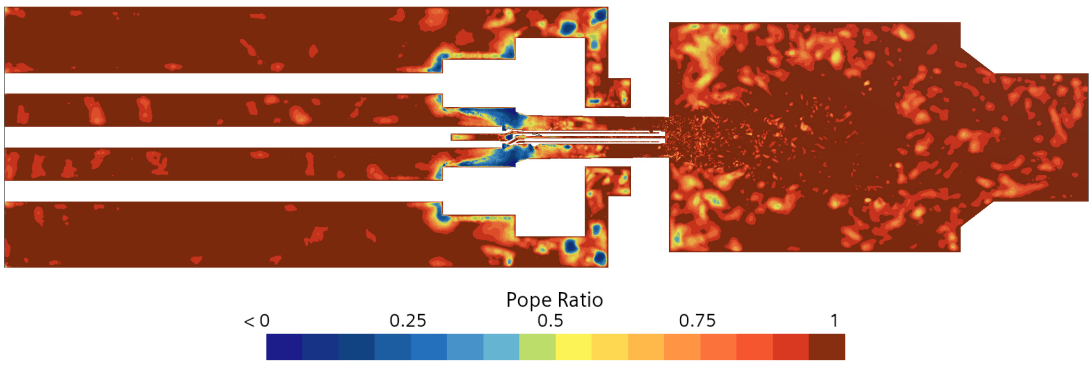

Figure 4.13: Pope criterion for LES quality.

4.5 Investigation of Combustion Models

Two different combustion models i.e. flamelet (FGM) and complex chemistry (LFC) methods are studied in LES using the FOI mechanism. Before running the LFC model using LES, it is first simulated using RANS. The temperature is very low at around 1600 K and oscillates, this means that it is very difficult to converge even using the less complex model.

Then, unsteady RANS is applied and the temperature gradually increases to 1800 K. However, when the model is switched to LES, the temperature drops drastically back to around 1600 K as shown in Figure 4.14. Moreover, it can be seen in Figure 4.15 that the outlet temperature obtained with LFC is significantly lower than with in FGM.

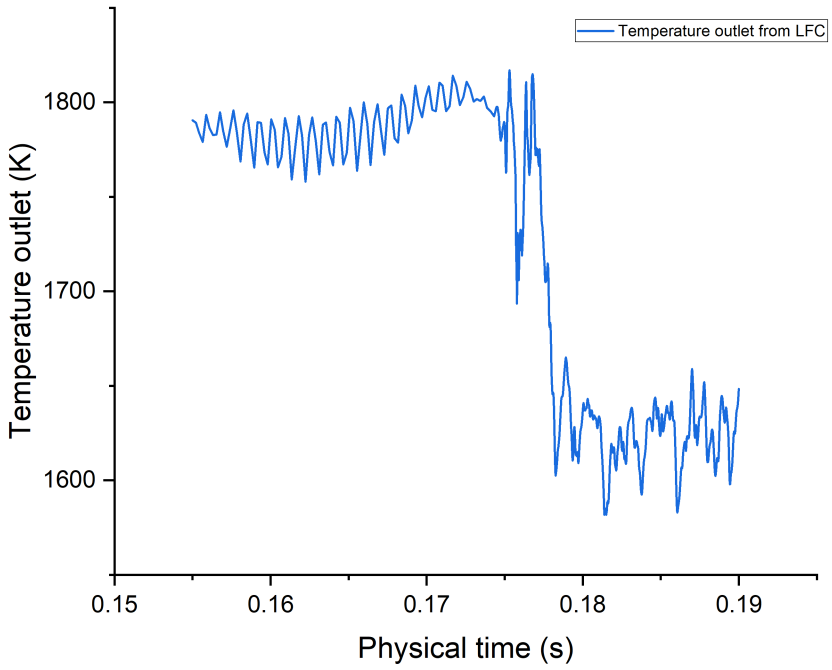

Figure 4.14: Dipping of temperature outlet when switching for the RANS to LES from LFC case.

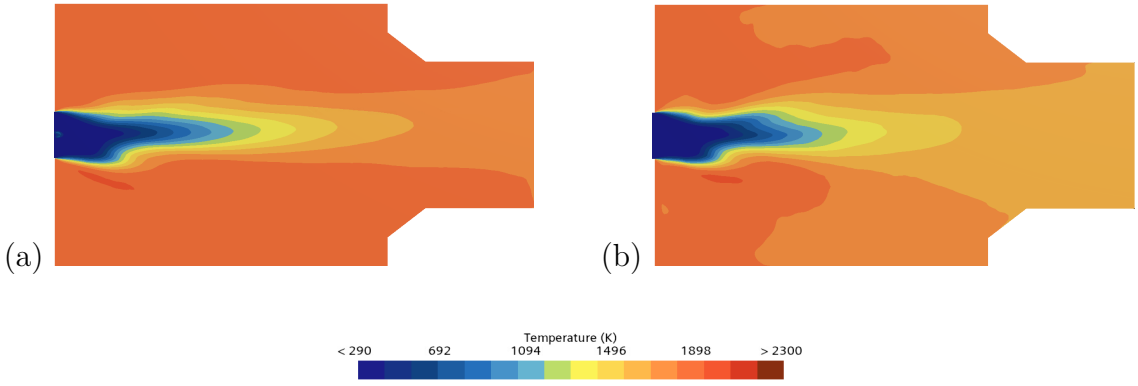

Figure 4.15: Comparison of the temperature fields obtained from FGM (a) and LFC (b).

This huge temperature drop when switching from RANS to LES and the differences of exit temperature between these two models may be caused by the time taken to converge since it can be seen in the exit temperature plot, Figure 4.16, that the temperature from LFC is still rising. There are two main points to be considered involving time step and geometry. A fairly small time step is required. The burner geometry provides complex fuel injection at a high Mach number which is around 1 at the fuel jet area and this requires sufficient low time step to achieve Courant

Number approaching 1 to balance stability and accuracy, ensuring that the simulation proceeds efficiently while capturing the essential dynamics of the system. Another point is the geometry expansion. When the field switches from RANS to LES, the jet flow of fuel attempts to drive out the air and fill up dead corners, then, the temperature rises again when mixing and burning start to take place. The massive volume expansion ratio of of the flow coming from the jet inlet to the chamber requires a substantial duration to flush the hot gas around the corner to reach the exit plane. This argument supports the dipping in temperature in LFC case because temperature is directly affected by the degree of mixing as it is a diffusion flame.

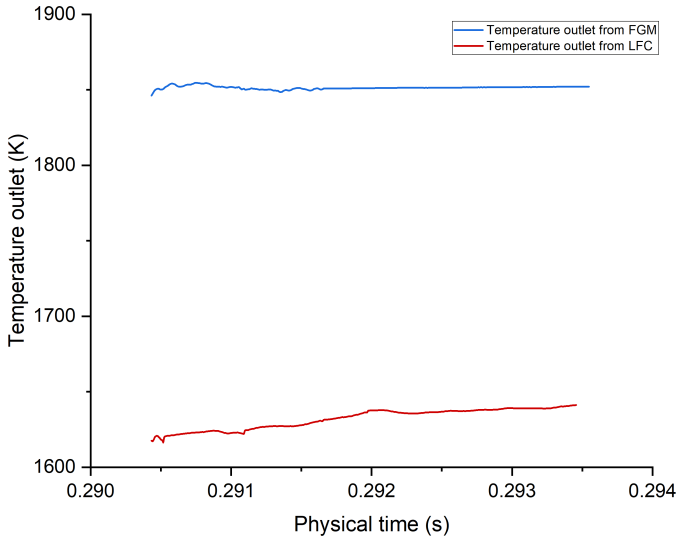

Figure 4.16: Comparison between the exit temperature from FGM (blue) and LFC (red).

To further assure these assumptions, the crucial parameters such as mixture fraction, hydrogen and water mass fraction at the exit are evaluated and compared. The mixture fraction is shown in Figure 4.17 and it reveals that mixing occurs faster in FGM model. Besides, the mass flow averaged of mean mass fraction and mass flow rate of water at the exit are calculated and compared. The amount of water is expected to be higher with the case that results higher flame temperature since the main product of hydrogen combustion is water. FGM yields higher amount of water which is 2.2 g/s while LFC delivers 1.7 g/s, therefore higher temperature is reached in FGM. This information supports the assumptions of the difficulty to converge due to the volume expansion and time step as discussed earlier.

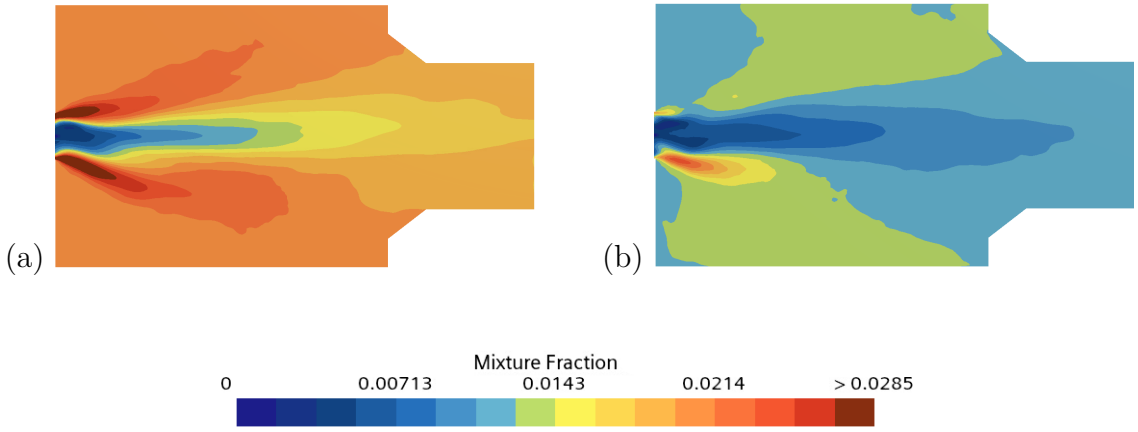

Figure 4.17: Comparison of the mixture fraction field obtained from FGM (a) and LFC (b).

Another key point to be discussed is the combustion model. LFC is one of the complex chemistry models that demands much longer time to converge compared to FGM as it involves a detailed description of the chemical kinetics. Solving the partial differential equations for all species and reactions is computationally intensive. In contrast, FGM method simplifies the chemical kinetics by precomputing a reduced set of representative flamelet solutions that describe the essential behavior of the flame.

4.6 Comparison between Simulation and Experimental results

The simulation results from RANS and LES using FOI mechanism and FGM combustion model with the same equivalence ratio of 0.615 are compared with experimental result [18].

In term of temperature, the exit temperature from RANS fluctuates within the range of 1850 to 1890 K. For LES, it is 1850 K as demonstrated in Figure 4.12 which is considerably close to the adiabatic temperature around 1858 K. For the experiment, it is widely acknowledged that the flames can reach extremely high temperature and often exceeding the limit of the thermocouple and different region of the flame can have significantly different temperatures, making it difficult to obtain a single representative measurement. Hence, flame temperature measurements often rely on indirect methods, such as analyzing the emitted radiation spectrum or using computational models to estimate the temperature distribution within the flame. In this case, the temperature reference to compare with the simulation attained from calculating adiabatic flame temperature using chemical kinetic software such as Cantera and the flame temperature at this equivalent ratio. Regarding flame shapes, temperature field acquired from the simulations and experiment are illustrated in Figure 4.18.

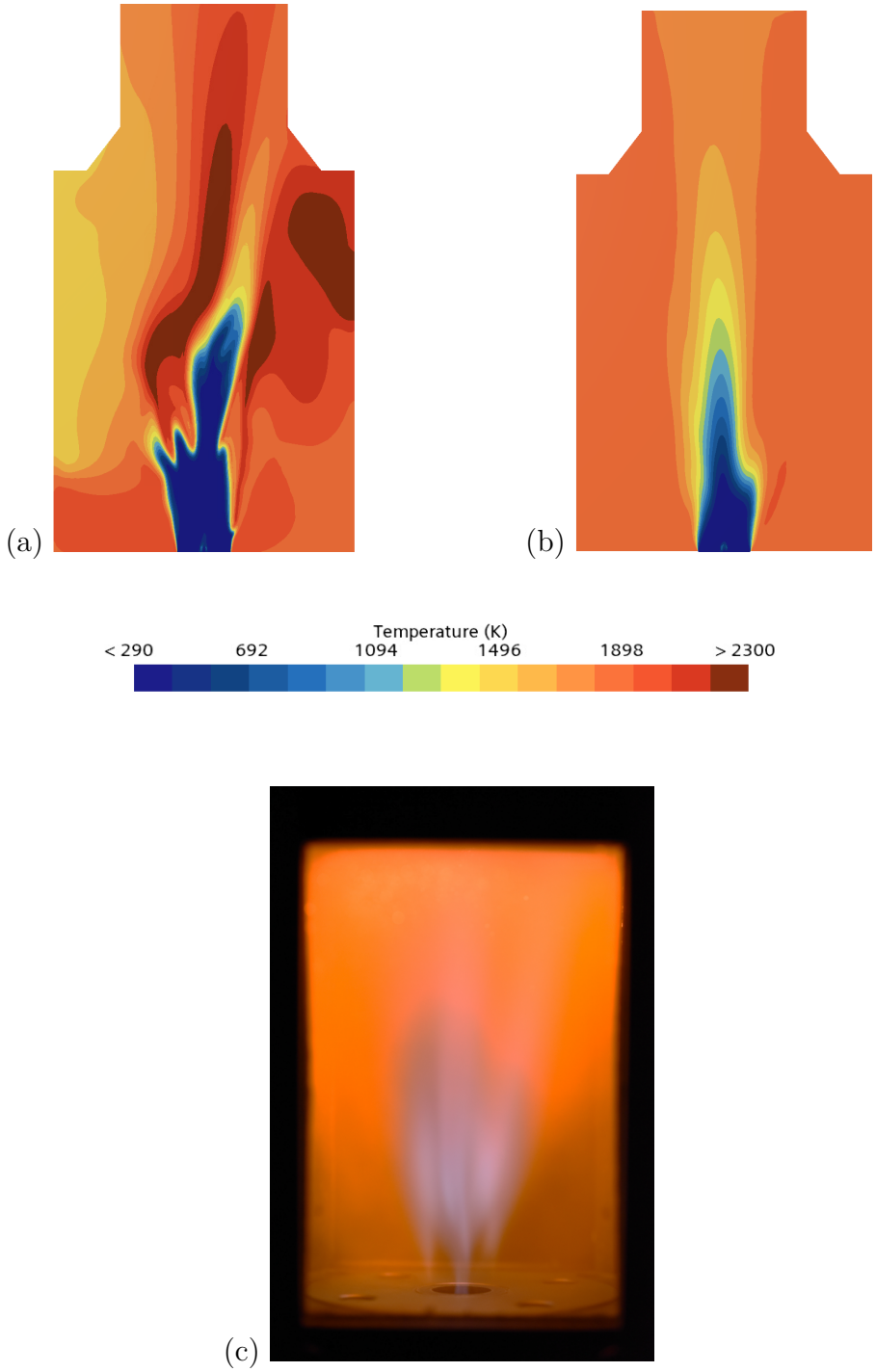

Figure 4.18: Comparison of flame shapes attained from RANS (a), LES (b), experiment (c).

The inner zone primarily contains unburnt fuel where is relatively cool and often appears bluish in color. The length of this inner zone is measured for each case and they are 7.38, 7.05, and 7.47 cm for RANS, LES, and experiment, respectively. For the reaction zone, it is the region where the fuel and oxidizer mix and combustion occurs. It is typically characterized by high temperatures and bright yellow or orange and commonly recognized as a flame front. It is challenging to accurately identify this area since the flame front is not a static, uniform surface but a dynamic, constantly changing region where the fuel and oxidizer mix and combustion occurs. This variability makes it difficult to capture precise measurements. Beyond the reaction zone, the flame temperature decreases, and the combustion products mix with the surrounding air. Reflecting on these zones and temperature distribution shown in Figure 4.18 it can be justified that the flame shape from the simulations represent the one from the experiment. Furthermore, this comparison implies that RANS is sufficient and effective to predict the result for this flow regime and boundary condition with substantially less computational consumption.

5

Conclusion

Hydrogen is one of the most promising alternative fuels for the gas turbines to drive zero emissions, hence it is important to study the effect of its usage so that proper modification can be conducted accordingly. In this study, the investigation of numerical methods for pure hydrogen combustion using a micromix combustor for industrial gas turbines with different chemical mechanisms, turbulence and combustion models is performed and compared. The domain and mesh are generated and refined strategically focusing on the crucial area around the fuel and where jet cross flow and mixing occurred. The mesh sensitivity is established and the mesh used in this study is validated to provide sufficient accuracy and contains 21 million cells. The asymmetry is discovered and it is convinced to be a result of the physics and geometry.

After the mesh is validated, three different RANS models including LagEB $k-\varepsilon$, standard $k-\varepsilon$, and SST $k-\omega$ are studied. It can be concluded that LagEB $k-\varepsilon$ provided the most promising result by considering the temperature at the exit and flow field across the combustor. Meanwhile, the exit temperature delivered from standard $k-\varepsilon$ noticeably deviates from the adiabatic temperature at 1858 K which was obtained from the chemical kinetics tool and the case using SST $k-\omega$ model faces difficulty to converge. To balance the accuracy and computational resources, LagEB $k-\varepsilon$ is selected to study further. The selection of chemical mechanism is then investigated by varying three kinetics involving GRI FOI and NUIG. The results obtained from these mechanisms are as expected for both temperature and flow fields. They are also considered to be indistinguishable and this can be explained by similar reactive species, reaction pathways and combustion phenomena. Additionally, they are extensively validated against experimental data at atmospheric condition. Despite all mechanisms being proven to give comparable results, FOI mechanism is chosen to examine further due to the least number of reactive species to ensure simulation efficiency.

The comparison between RANS LagEB $k-\varepsilon$ and LES using the same combustion model (FGM) and mechanism (FOI) shows some differences in flame characteristic in term of hot spot formation. The RANS model produces hot spots which is possibly due to inaccuracies in predicting turbulent transport, underestimation of turbulent kinetic energy dissipation, and inadequate grid resolution. These factors can lead to erroneous temperature and concentration gradients. The exit temperature from the RANS model is unstable and slightly higher than from the LES model (1850 K), reflecting these issues. The LES model, which resolves 96% of turbulent

kinetic energy, demonstrates its superior capability in preventing hot spot formation and provides more reliable temperature predictions.

Thereafter, different combustion models consisting of flamelet and reacting species transport are studied. FGM kinetic rate and laminar flame concept are selected for FGM and complex chemistry model accordingly. The flame temperature is witnessed to be extremely low in LFC case which is around 1600 K. However, the results from RANS and LES are expected to be equivalent when assigning the same boundary conditions. In this case, differences between these two models can be described as a matter of time to reach convergence because the exit temperature generated from LFC is still increasing consistently. Two main factors causing this initial deviation are small time step and geometry. When transitioning to a transient model, the complex jet flow induced by the geometry necessitates a significantly smaller time step, coupled with a substantial volume expansion of the chamber. This causes LES simulations to take considerably longer to progress and converge compared to RANS. Additionally, the use of complex chemistry significantly contributes to the extended time required for the simulation to reach convergence. The increased complexity of the LFC model demands higher computational resources, as it involves solving a large number of equations. Nevertheless, the exit temperature from the LFC shows an upward trend towards the desired temperature, similar to the behavior observed in FGM.

Lastly, the results from simulation and experiment are compared. It can by summarized that RANS LagEB $k-\varepsilon$ is effective in predicting accurate flame shape, temperature and flow fields when validated against the experiment with substantially low computational consumption compared to LES. In summary, the key findings from this study are the appropriate numerical methods to predict hydrogen combustion flame in a micromix combustor. Applying RANS LagEB $k-\varepsilon$ model is considered to be a reliable model which balances accuracy and cost and is suitable to predict turbulence for industrial applications.

6
Future Work

Hydrogen combustion in gas turbines represents a promising advancement in the pursuit of sustainable and clean energy solutions and a micromix combustor is a potential design to cope with the undesired phenomena caused by unique properties of hydrogen, for instance, flashback. Moreover, hydrogen combustion is still in a developing phrase, thus, there are several areas to be studied and improved further. Comparison of the simulation results with experiment data when available is strongly suggested. For this study, three main areas are recommended to continue comprising geometry, boundary conditions, stability and NOx formation.

For the geometry, the number and size of the injector should be carried to investigate the effect of the design on flame shapes and interactions. Modification of geometry can greatly contribute to mixing which directly affects the combustion. The flame characteristics can be altered according to the volume of the combustion chamber by adjusting cross-sectional area or length of the chamber. The chamber is suggested to be extended so that the effect from the upstream can be excluded at the exit.

Boundary conditions are one of the most interesting points to study. The equivalence ratio can be adjusted to optimize the flame temperature. The operating pressure at real conditions used in gas turbines should be further studied. Thermoacoustic phenomena should be investigated to ensure system stability by evaluating relevant parameters and mechanisms such as combustion dynamics, acoustic resonance, and heat transfer.

It is crucial to explore NOx formation. In hydrogen combustion, it primarily occurs through thermal NOx mechanisms due to the high flame temperatures and the possibility of hot spots. Prompt NOx formation and fuel NOx are relatively minor contributors. Understanding these mechanisms is essential for developing strategies to mitigate emissions.

Bibliography

[1] Energy Institute. (n.d.). Resources and data downloads. Statistical Review of World Energy. https://www.energyinst.org/statistical-review/resources-and-data-downloads

[2] Rogelj, J., Elzen, M. D., Höhne, N., Fransen, T., Fekete, H., Winkler, H., Schaeffer, R., Sha, F., Riahi, K., Meinshausen, M. (2016). Paris Agreement climate proposals need a boost to keep warming well below 2 °C. Nature, 534(7609), 631–639. https://doi.org/10.1038/nature18307

[3] Schmidt, O., Gambhir, A., Stafell, I., Hawkes, A., Nelson, J., Few, S.: Future cost and performance of water electrolysis: an expert elicitation study. Int. J. Hydrogen Energy (2017). https://doi.org/ 10.1016/j.ijhydene.2017.10.045

[4] M. Boyce, Gas Turbine Engineering Handbook, Butterworth-Heinemann, 2011.

[5] Soares C. Gas Turbines: A Handbook of Air, Land and Sea Applications;.

[6] Boyce MP. Gas turbine engineering handbook. Oxford : ButterworthHeinemann;.

[7] Zhou, H., Xue, J., Gao, H., Ma, N. (2024). Hydrogen-fueled gas turbines in future energy system. International Journal of Hydrogen Energy, 64, 569–582. https://doi.org/10.1016/j.ijhydene.2024.03.327

[8] Funke, H., Beckmann, N., Abanteriba, S. (2019). An overview on dry low NOx micromix combustor development for hydrogen-rich gas turbine applications. International Journal of Hydrogen Energy, 44(13), 6978–6990. https://doi.org/10.1016/j.ijhydene.2019.01.161

[9] Moell, D. (2018). Modelling of methane and hydrogen enriched methane flames in industrial gas turbine burners.

[10] Andersson, B., Andersson, R., Håkansson, L., Mortensen, M., Sudiyo, R., Van Wachem, B. (2011). Computational Fluid Dynamics for Engineers. https://doi.org/10.1017/cbo9781139093590

[11] Cant, R. S., Mastorakos, E. (2007). An introduction to turbulent reacting flows. In PUBLISHED BY IMPERIAL COLLEGE PRESS AND DISTRIBUTED BY WORLD SCIENTIFIC PUBLISHING CO. eBooks. https://doi.org/10.1142/p498

[12] S. Lardeau and F. Billard, "Development of an elliptic-blending lag model for industrial applications.," 54th AIAA Aerospace Sciences Meeting, 2016.

[13] D. C. Wilcox, Turbulence Modeling for CFD, DCW Industries, 1998

[14] M. Frenklach, H. Wang, C.-L. Yu, M. Goldenberg, C.T. Bowman, R.K. Hanson, D.F. Davidson, E.J. Chang, G.P. Smith, D.M. Golden, W.C. Gardiner and V. Lissianski,

[15] M. Frenklach, H. Wang, M. Goldenberg, G.P. Smith, D.M. Golden, C.T. Bowman, R.K. Hanson, W.C. Gardiner and V. Lissianski, 'GRI-Mech—An Optimized Detailed Chemical Reaction Mechanism for Methane Combustion,' Report No. GRI-95/0058, November 1, 1995.

[16] Zettervall, N., Fureby, C. A Computational Study of Ramjet, Scramjet and Dualmode Ramjet Combustion in Combustor with a Cavity Flameholder. In: 2018 AIAA Aerospace Sciences Meeting. 2018. p. 1146.

[17] combustion and chemistry center, University of Galway : NUIGMech1.1, Reaction Mechanism (2020), https://www.universityofgalway.ie/combustionchemistrycentre/mechanismdownloads/

[18] Durocher, A., Fan, L., Francolini, B., Furi, M., Bourque, G., Bergthorson, J. M., Yun, S., Vena, P. Characterization of a novel AM micromix nozzle burning methane to hydrogen. Proceedings of ASME Turbo Expo 2023, Boston, USA, 2023. GT2023-104117

[19] Arthur, H., Lefebvre and Ballal Dilip R., Gas Turbine Combustion Alternative Fuels and Emissions, Third edition © by Taylor and Francis Group, LLC CRC Press is an imprint of Taylor Francis Group, an Informabussines, 2010.

[20] Exploring the Courant–Friedrichs–Lewy Condition in CFD | Resolved Analytics. (n.d.). Resolved Analytics. https://www.resolvedanalytics.com/cfd-in-practice/what-is-the-courant-friedrichs-lewy-cfl-condition-in-cfd

[21] Lu, Z., Piro, M., Christon, M. (2022). Mesh and turbulence model sensitivity analyses of computational fluid dynamic simulations of a 37M CANDU fuel bundle. Nuclear Engineering and Technology, 54(11), 4296–4309. https://doi.org/10.1016/j.net.2022.06.004

[22] Sadiki, A., Maltsev, A., Wegner, B., Flemming, F., Kempf, A., Janicka, J. (2006b). Unsteady methods (URANS and LES) for simulation of combustion systems. International Journal of Thermal Sciences, 45(8), 760–773. https://doi.org/10.1016/j.ijthermalsci.2005.11.001

[23] Sidik, N. a. C., Yusuf, S. N. A., Asako, Y., Mohamed, S. B., Japa, W. M. a. A. (2020b). A short review on RANS turbulence models. CFD Letters, 12(11), 83–96. https://doi.org/10.37934/cfdl.12.11.8396

[24] Boivin, P. (2012). Reduced-kinetic mechanisms for hydrogen and syngas combustion including autoignition. Reduced-kinetic Mechanisms for Hydrogen and Syngas Combustion Including Autoignition.

[25] Yousefian, S., Quinlan, N. J., Monaghan, R. F. (2018). Simulation of turbulent flow in a rapid compression machine: Large Eddy Simulation and computationally efficient alternatives for the design of ignition delay time experiments. Fuel, 234, 30–47. https://doi.org/10.1016/j.fuel.2018.06.117

DEPARTMENT OF SOME SUBJECT OR TECHNOLOGY
CHALMERS UNIVERSITY OF TECHNOLOGY
Gothenburg, Sweden
www.chalmers.se

CHALMERS
UNIVERSITY OF TECHNOLOGY